2015

Experimental Study of a Flying Wing Anchor in Sand Under Pure Loading

Sven Sivarajah
University of Rhode Island, sven.sivarajah@gmx.de

EXPERIMENTAL STUDY OF A FLYING WING ANCHOR IN SAND UNDER PURE LOADING

BY

SVEN SIVARAJAH

A THESIS SUBMITTED IN PARTIAL FULFILLMENT OF THE

REQUIREMENTS FOR THE DEGREE OF

MASTER OF SCIENCE

IN

CIVIL AND ENVIRONMENTAL ENGINEERING

UNIVERSITY OF RHODE ISLAND

2015

MASTER OF SCIENCE THESIS

OF

SVEN SIVARAJAH

APPROVED:

Thesis Committee:

Major Professor Aaron S. Bradshaw

Christopher D.P. Baxter

David Taggart

Nasser H. Zawia
DEAN OF THE GRADUATE SCHOOL

UNIVERSITY OF RHODE ISLAND
2015

ABSTRACT

The Flying Wing Anchor is a new anchor concept that stabilizes offshore foundations for renewable energy. The anchor, with a wing-like shape, uses its weight to penetrate into the seabed by free-fall and mobilizes its full capacity by using the in-service load, so it is a new concept to optimize the sustainability of offshore foundations for renewable energy. A major challenge is to understand the trajectory of the anchor during loading because the anchor capacity depends on the final embedment depth and orientation. The objective of this study is to experimentally investigate the anchor behavior under pure static loading conditions that ultimately could be used to assess the anchor trajectory through an analytical model. Physical model tests were performed on the Flying Wing Anchor for four modes of pure loading: in-plane shear vertical, normal vertical, pitch rotation and in-plane horizontal. The results were used to calculate dimensionless bearing factors for each failure mode. The bearing factors ranged from 2 to 18 depending on the pure loading mode for embedment ratios between 1 and 4.

ACKNOWLEDGMENTS

This past year has been one the most interesting and exciting, both personally and professionally.

This thesis would not have been possible without my Major Professor, Dr. Aaron Bradshaw. I would like to thank you for your support, patience, inspiration, pure enthusiasm, encouragement and advice throughout my thesis and research.

In addition, I would like to thank Joseph Giampa for his help and input towards this research and throughout my studies and Kevin Broccolo for assisting throughout my research. I would further like to extend my appreciation out to Dr. Christopher Baxter for providing me knowledge and insight throughout my graduate studies.

I also would like to address my thanks to everyone who has been a part of my studies and contributed to it in any possible way and I feel grateful.

Finally, I would like to thank my wonderful, loving and supportive family. To my parents, Srimathi Hemalatha Sivarajah and Suppiah Sivarajah, for always been there, helping me strive to be the best I can be, and for making me a good person. For my Father for given me great opportunities. For my Mother, thank you for your unconditional support, love, and showing me Buddhism without I never be as good and thankful as I am now. I love you Amma and Appa and I miss you everyday Appa. Thank you to my sister, Chanuska, and my brother, Stephan, for you support, fun and

for always being there. Without you four I would not be the same person I am today. The things you did for me and the lessons and morals you taught me are comparable with no one. Thank you.

TABLE OF CONTENTS

LIST OF TABLES

LIST OF FIGURES

FIGURE PAGE

CHAPTER 1: INTRODUCTION

Increasing emission of carbon dioxide from combustion of fossil fuels and the lack of resources is the reason why there is a need for continued research in renewable energy. Wind energy is one of the most sustainable and environmental friendly energy solutions available.

Onshore wind farms already provide a great supply of electric power (Matha et al., 2009). Offshore wind farms are also appealing because of the vast wind resources that are available offshore (Musial et al. 2004). Manufacturers use land-based turbines with upgraded electrical and corrosion control for offshore areas (Butterfield and Musial, 2004). Offshore wind farms have already been constructed in Europe and Asia and the first US installation is planned for construction in August 2015 in Rhode Island.

Fixed bottom structures are typically used in shallow water depths (i.e. < 30 m). Fixed structures include monopiles, lattice-jacket, and tripods. The use of these foundation systems is expensive and impractical in deeper water. The use of floating platforms is a more economical way to stabilize offshore platforms in deep water. Floating structures have already been used in the offshore oil and gas industry.

Floating platforms are stabilized or fixed with anchor systems. The development of floating systems for deep-water offshore installations has placed greater demand on anchoring systems. Over the years, various anchoring systems and designs have been

proposed and used. They differ by the way they achieve stability and resistance against the applied forces. The most common are catenary moorings, taut-leg moorings, and vertical tension legs (Figure 1). The main advantage of taut or semi-taut systems is that they have smaller scopes, they have a smaller footprint than catenary systems, and they require less anchor line. In taut mooring systems the anchor has to withstand both horizontal and vertical forces. Inclined, vertically loaded plate anchors, pile anchors, and torpedo anchors for example are used, while drag embedment anchors are typically used for catenary mooring systems. (Randolph and Gourvenec, 2011; Musial et al., 2004; TU Delft, 2005).

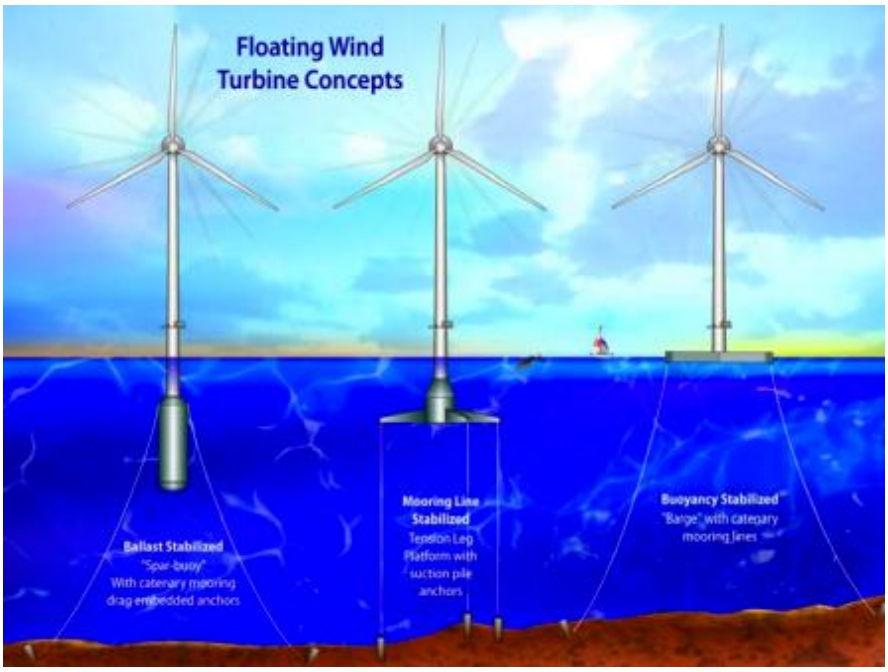

Figure 1. Catenary mooring system (left and right) and vertical tension leg system (middle) (adapted from Butterfield et al. 2007).

Plate anchors for taut and semi-taut mooring system achieve their capacities, i.e. resistance, from bearing on the soil. Plate anchors in general have the ability to achieve very deep embedment depths. The anchors are mostly used in clays, where anchor manufacturers such as Vryhof Anchors (2010) developed design charts and Equations to calculate the capacities. To achieve deep embedment depths in sand, plate anchors must be been driven or jetted in place (NAVFAC, 2012).

Colleagues at the University of Texas, University of Rhode Island, Queens University of Belfast, and University College Dublin have proposed a new concept called the "Flying Wing" anchor (patent pending) (Gilbert and Bradshaw, 2012). The anchor, with a wing-like shape, uses its weight to penetrate into the seabed by free-fall. It is a new concept to improve the sustainability of offshore foundations for renewable energy, because these anchors use their self-weight for installation, are a self-improving foundation that uses the in-service loads to mobilize its full capacity. They can also be reused. The Flying Wing Anchor maximizes efficiency by drawing from the best attributes of torpedo piles and plate anchors. The research on a new anchor concept was needed because offshore wind energy is very expensive and it was needed to bring the cost down to become competitive.

The installation technique for the Flying Wing Anchor is comparable to torpedo pile anchors. The Flying Wing Anchor, transmitted by a long chain or cable, is dropped from above the sea floor with its nose facing down and penetrates vertically the soil like a torpedo pile. By increasing the tension the anchor moves along a specific

trajectory till it reaches the expected soil depth at a certain orientation like a plate anchor (Figure 2) (Gilbert and Bradshaw, 2012).

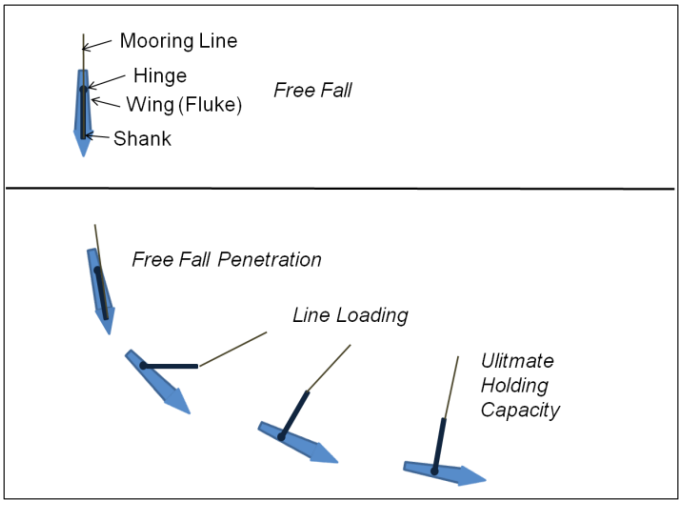

Figure 2. Flying Wing Anchor during penetration and loading (Gilbert and Bradshaw, 2012).

The development of the Flying Wing Anchor requires the study of installation kinematics and pullout capacity. The University of Texas is focusing on experimental and analytical studies of the anchor in clay. University College Dublin is performing numerical analysis on the anchor in clay. Rate effects in clay are being explored at Queens University Belfast. The University of Rhode Island is focusing on the feasibility of the Flying Wing Anchor in sand. This includes studies on the free-fall penetration (Breithaupt, 2015) and capacity (Dietrich, 2014). This thesis focuses on the trajectory aspects of the anchor kinematics.

The ultimate challenge is to be able to predict the final embedment depth and

orientation of the anchor below the seafloor because these aspects will affect capacity. A first step to understanding the kinematics is to understand the resistance of the anchor under pure static loading. The objective of this thesis was therefore to experimentally determine the resistance of the Flying Wing Anchor to four loading modes illustrated in Figure 3. This includes in-plane shear (vertical fluke) where the load is parallel to the fluke and the plate is vertical (Figure 3a), normal (vertical fluke) (Figure 3b) where the load is perpendicular to the fluke and horizontal, pitch rotation (vertical fluke) (Figure 3c), and in-plane shear (horizontal fluke) (Figure 3d) where the load is parallel to the fluke and horizontal. The experimental work is a starting point for the development of an analytical model that will be able to predict the complete trajectory of the anchor.

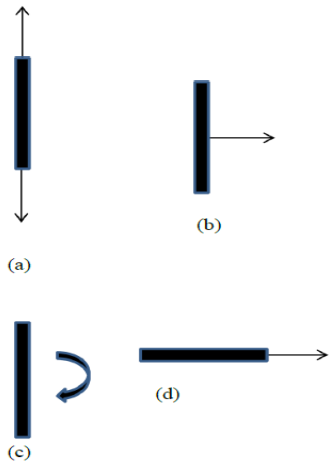

Figure 3. Penetration modes: (a) in-plane shear (vertical fluke), (b) normal (vertical fluke), (c) pitch rotation (vertical fluke) and (d) in-plane shear (horizontal fluke).

This thesis contains four remaining chapters. Chapter 2 presents a review of the literature related to the kinematic behavior of plate anchors to gain knowledge for further research on the Flying Wing Anchor. Chapter 3 discusses the physical modeling methods. Chapter 4 discusses and shows the results of the physical modeling efforts. Chapter 5 presents the major findings as well as recommendations for further research.

CHAPTER 2: LITERATURE REVIEW

The following section will discuss the relevant literature and studies that have been carried out to determine the kinematic behavior and trajectory of plate anchors in sands. The review includes the kinematic behavior of plate anchors, and a synthesis, which explains also the use of bearing factors for the analytical model that predicts the complete trajectory.

2.1 KINEMATICS OF EMBEDDED PLATE ANCHORS

Le Lievre and Tabatabaee (1981) discussed the problem of the holding capacity of marine anchors in cohesionless soil and the reason for the difference in the performance of drag embedment anchors and simple flat plates. The authors explained the general behavior of anchor-mooring cable systems in soil, the role which the various anchor components play during the embedding process and a method of analysis to compute the approximate holding capacity and acting forces on the anchor components. The study focused on anchors with a moveable planar fluke surface. Laboratory and field-testing were performed. The tests and the method of analysis showed that it was possible to predict the relationship between holding capacity and depth of penetration for anchors embedded in sand with reasonable accuracy. Also the forces acting on the shank and fluke could be estimated. By testing the anchors with different fluke angles it appeared that there are 2 factors involved in the optimization of anchor performance. The first is the fluke angle to achieve the maximum burying force (35° for the D-19 Danforth anchor). The second is the anchor geometry to

maintain rotational stability while minimizing the resistance to penetration of the shank and stock (Figure 4).

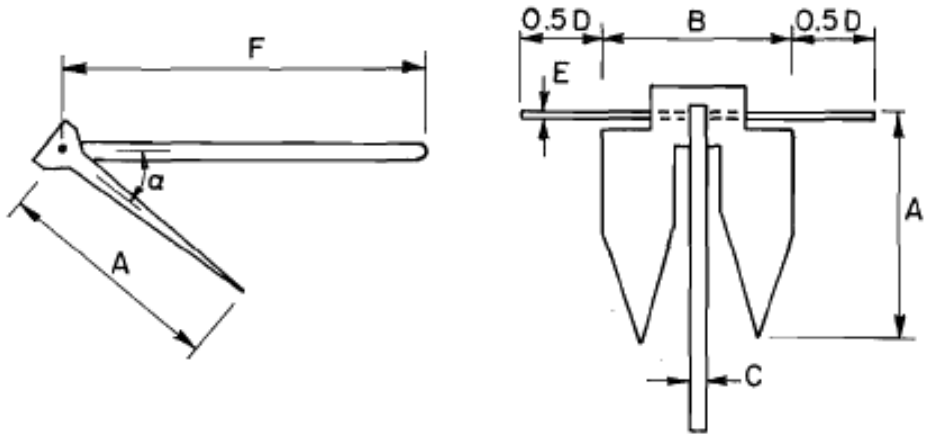

Figure 4. Fluke angle and anchor geometry (adapted from Le Lievre and Tabatabaee, 1981).

Le Lievre and Tabatabaee suggested that there is no force acting on the back the fluke. The expected maximum depth to which an anchor penetrates the soil by continued dragging could not be predicted. The authors explained that it is possible to compute a value of the holding capacity for an anchor, which has been placed at a particular depth, there will generally be a limit to the depth of embedment which can be achieved by a pulled anchor. The holding capacity of an anchor cannot be specified in general without giving due consideration to the depth-penetration resistance characteristics of the shank-stock-cable system (Figure 5 and 6).

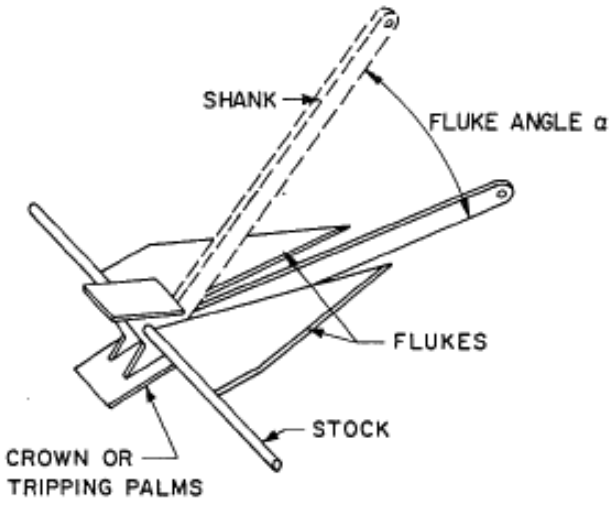

Figure 5. Typical anchor with planar flukes (adapted from Le Lievre and Tabatabaee, 1981).

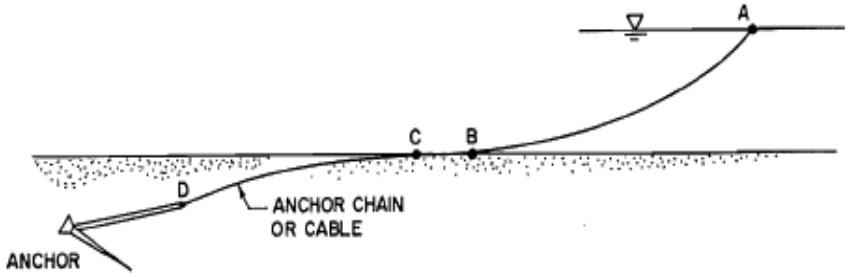

Figure 6. Anchor-mooring cable system (adapted from Le Lievre and Tabatabaee, 1981).

The ultimate holding capacity and the expected maximum depth could not be estimated during their studies, but a relationship between these two could be predicted. The authors indicated that additional studies were required to estimate the resistance to burial of the anchor components, specifically the shank, stock, and towing cable (Figure 6).

Neubecker and Randolph (19996a) studied the kinematic behavior of drag embedment anchors during embedment in sand. Two aspects of the drag anchor behavior were focused on. The first is the static resistance of the drag anchor (Neubecker and Randolph, 1996b) and the second is the kinematic behavior of the drag anchor or how the anchor will move when subjected to a chain (cable) load that exceeds the anchor´s current capacity as calculated in the static analysis. For the static analysis four forces on the anchor were regarded: the chain force, forces on the back and front of the fluke, and a force on the shank (Figure 7). The equilibrium of the anchor allows for the calculation of all forces. The resulting implication is that the back of the fluke must move in the direction of its plane (More information in Neubecker and Randolph, 1996b). For the kinematic behavior, the drag anchor and the soil are assumed to be two rigid bodies that move in some kinematically admissible manner. Neubecker and Randolph explained that the kinematics of the system could be fully described by three conditions of anchor and soil displacements. The first condition that has to be satisfied is the displacement of the anchor (du_a) is generally parallel to the back of the fluke. If the force on the back of the fluke becomes zero, this condition lifts and the anchor is free to travel away from the soil behind it. The second condition is that the displacement of the soil relative to the anchor (du_{sa}) must be in the direction of the upper face of the fluke. The last condition is that the soil wedge displacement (du_s) will be inclined at the dilation angle to the failure surface. All conditions are supported by experimental tests (Figure 7).

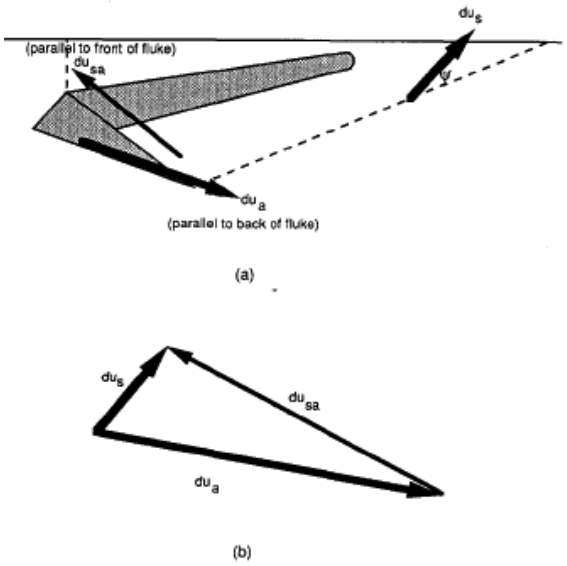

Figure 7. Kinematics of the anchor-soil displacement: (a) absolute and relative displacements, (b) final displacement diagram (adapted from Neubecker and Randolph, 1996a).

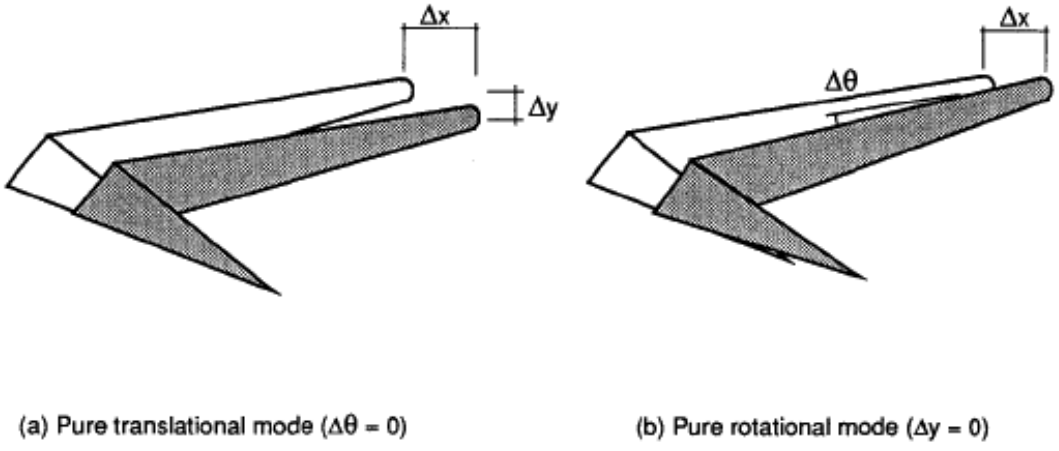

Figure 8. Modes of incremental anchor displacement (adapted from Neubecker and Randolph, 1996a).

The anchor displacement prediction method was developed around a minimum work approach through the synthesis of static and kinematic behavior. Through series of assumed displacements and rotations, the set, which dissipates the least amount of work, can be tested and seen. The authors found out that the anchor takes the path with the least resistance. In each step the anchor is simulated by moving the anchor some finite displacement (Δx) and assuming that it responds by penetrating and rotating by Δy and $\Delta\theta$ (Figure 8). Neubecker and Randolph examined this hypothesis through model test data and show a successful framework for predicting the full embedment history of drag anchors in sand. To obtain good penetration and hence holding capacity, the shank resistance has to be minimized. The authors found out that the movement of the anchor can be assumed well by assuming that the anchor travels in the direction of the back of the fluke. The synthesis of static and kinematic behavior has enabled the development of a framework that provides an approach to modeling theoretically the embedment and holding capacity of drag anchors in sand.

Neubecker and Randolph (1996b) discussed the static equilibrium of drag embedment anchors during embedment in sand. A limit equilibrium method was developed to allow the anchor holding capacity to be predicted given a specific anchor geometry and position relative to the free surface of the sand. A series of centrifuge model anchor tests were performed in silica and calcareous sands. The comparison between the static capacity of the anchor during embedment and the static equilibrium solution showed good agreement. The new method was developed to predict the pre-ultimate anchor capacities. The limit equilibrium solution showed good agreement with

experimental results. The method is based on that of Le Lievre and Tabatabaee (1981), but is more realistic by using a three dimensional failure pattern in the soil and a force acting on the back of the fluke (Figure 9).

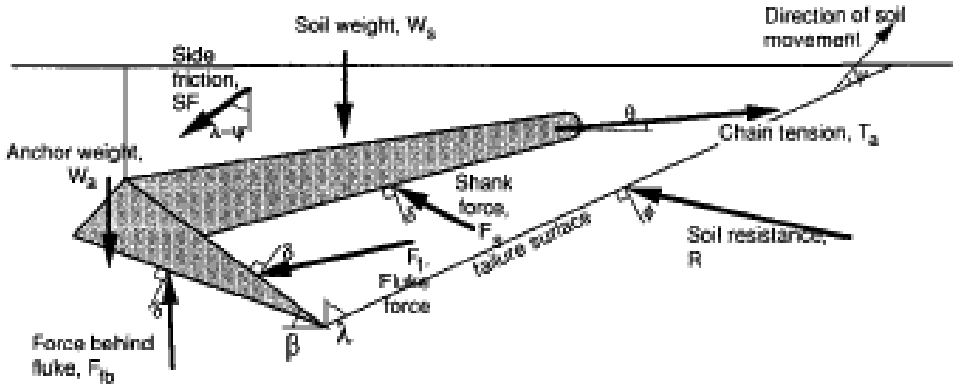

Figure 9. Overall anchor equilibrium by using a three dimensional failure pattern and force behind the fluke (adapted from Neubecker and Randolph, 1996b).

A failure wedge developing in front and to the side of the anchor then determines the static capacity of the anchor (Figure 10).

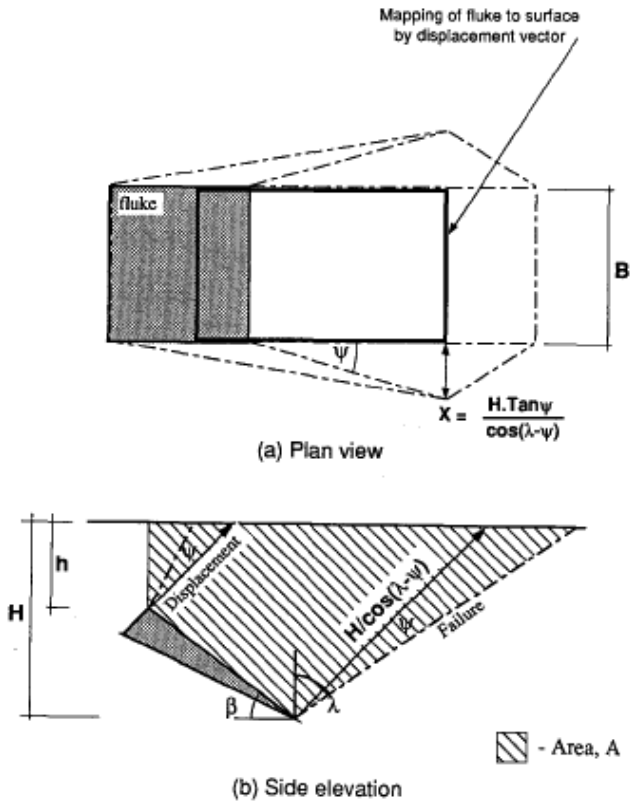

Figure 10. Three-dimensional failure mechanism in sand (adapted from Vermeer and Sutjiadi, 1985; Neubecker and Randolph, 1996b).

The authors stated that this not sufficient to predict the complete performance of the anchor, but provide an essential framework for prediction of anchor capacity in homogenous sand and more complex, layered profiles.

Ruinen et al. (2002) showed various methods to determine the holding capacity and trajectory of drag embedment anchors in sand and clay. Various anchors manufacture developed design graphs and these are the most common methods. More recent are the development of predicting the anchor holding capacity and trajectory based on

geotechnical methods. Their methodology is described in six steps, based on the solution methods for the static capacity of the anchor, the mooring line profile and the anchor dynamics. Step one calculates the initial position of the anchor. Step two calculates the static capacity in this position. Step three calculates the profile of the mooring line in the seabed. Step four is to check if the anchor has reached the ultimate holding capacity (fluke is close to horizontal). Step five checks if the anchor can still penetrate further and calculate the new position and rotation. Last step is to repeat the steps 2, 3 and 4 until the ultimate holding capacity is reached. This methodology can be used for layered soil, sand and clay.

The Technical University Delft (2005) presented an analysis of the penetration behavior of drag embedment anchors in sand. The authors developed a theory to analyze and calculate the forces acting on the anchor before and during embedment. Their approach splits the analysis into four phases. Phase one explains the anchor when it arrives at the seabed (i.e., no penetration exists). By pulling the mooring line, the anchor will plow into the seabed with a maximum fluke angle. When the soil resistance increases in front of the fluke, it is easier for the anchor to penetrate than to plow the seabed. The second phase is about the starting of the penetration into the ground. The cutting theory of Miedema (1987) is used. The third phase begins when the fluke is completely covered by the sand and the shank will become an extra factor, which will increase the penetration resistance. Strip footing theory from Verruijt (1983) was used to determine the shank resistance. The maximum shank resistance acts when the complete shank is covered and penetrated. The fourth and final phase

begins when the shank and fluke are completely covered by the sand and when there is still no equilibrium and a part of the mooring line will penetrate the soil. The mooring line will cause additional penetration resistance. For the calculation, the cutting theory of Miedema (1987) was still valid for the fluke and for the shank, and the strip footing theory in Verrujit (1983) for the mooring line. The anchor will be stable when there is a balance between the vertical and horizontal forces on the anchor parts, which are covered by the sand. In phase two, three and four of the modeling, the holding capacity and trajectory can be determined, because in reality the pull force is known. The modeling and calculation part of phase three makes it possible to make a total force and moment balance to predict the trajectory of the anchor. The trajectory of the anchor during penetration can be predicted by using the relationship between the different forces and moments on the anchor. The trajectory will stop when all forces are in equilibrium or when the pull force is too high for that anchor at a certain depth (maximum holding capacity is reached).

Liu et al. (2010a) showed that the ultimate embedment depth (UED) is important to evaluate the performance of vertically loaded plate anchors (VLA) and it is also a key parameter in predicting the kinematic trajectory of VLAs. The authors show the analytical derivation to express the UED for clay and sand. The summary will focus on sand. When the anchor reaches the UED by the drag forces, the anchor fluke approaches an approximately horizontal orientation, so the movement direction of the fluke is nearly horizontal. Based on the research in clay, DNV (2002) stated that the UED is dependent on soil conditions, the type and size of the anchor, the anchors

fluke angle and the type and size of the anchor forerunner (cable). The parametric study of the authors showed parameters that influence the UED, e.g. the drag angle of the shackle θ gets bigger by increasing depth of the UED or the effective bearing width affects the UED as well. This paper also shows the analytical derivation to express the UED.

The UED can be solved through:

$$Z_{ued} = \Delta z + m + \sqrt{m^2 + 2m\Delta z} \quad (1)$$

where, Δz is the distance from the shackle to the plane of the anchor fluke, and Z_{ued} is the UED of the fluke, and

$$m = \frac{(m1A_b + m2A_s)}{(2b)} \quad (2)$$

$$m1 = \frac{KN_{qf}(\theta_a - \theta_m)^2}{[N_{qf}\cos(\theta_a - \theta_m)]} \quad (3)$$

$$m2 = \frac{(\theta_a - \theta_m)^2 \tan\delta_f}{[N_{qf}\cos(\theta_a - \theta_m)]} \quad (4)$$

where, K is the lateral soil pressure factor, N_{qf} is the bearing capacity factor, A_b is the total projected area of the anchor on to the plane perpendicular to the horizontal, A_s is the total shear area of the anchor along the horizontal, δ_f is the angle of the interface friction, θa is the drag angle to the top of the surface of fluke at the shackle, and θ_m angle of the top surface to the movement, and b is the effective bearing width of the

dragline. The authors performed also experimental tests. The experimental model was designed for vertical load anchors and consisted of four parts: the experimental flume, drag and retrieval system, measurement system, and drag mooring conversion system (Figure 11).

Figure 11. Experimental flume or test tank (left) and the used anchor model (right) (adapted from Liu et al., 2010a)

The comparison between the experimental and theoretical model demonstrated that the calculation results are close to the experimental data. These authors showed theoretical expressions for predicting the UED in clay and sand. The effectiveness and veracity of the theoretical expressions for predicting the UED have been preliminarily verified in the paper. The present theoretical expression should be considered to give an upper bound evaluation of the UED.

Liu et al. (2010b) investigated five fundamental problems, which are closely relevant to the penetration mechanism and kinematic behavior of vertically loaded plate anchors. The aforementioned problems were investigated in a model experimental

system through a specially designed multi-parameter measurement technique. The five fundamental problems are clearly obtained by analyzing the kinematic parameters and trajectories of the anchor. The five problems that are explored were i.) the effects of the initial orientation of the anchor, ii.) the effects of the shank angle, iii.) the penetration direction of the anchor, iv.) the relationship between the fluke orientation and the drag angle at the shackle, and v.) the relationship between the drag distance and the anchor displacement in the soil. Square plate anchors with four soft shanks were used. They showed that the initial orientation is not a main factor that influences the anchor behavior but plays an important role in helping the anchor to initially penetrate the soil. The data showed that the kinematic trajectory is very sensitive to the shank angle in both sands. They showed that the anchor moves parallel to its fluke surface. It was observed that the behavior of drag anchors is directly influenced by the embedded dragline. It was noticed that the total anchor displacement was always the largest one, but still close to the drag distance. The embedment efficiency in saturated sand is better than in unsaturated sand. Under identical test conditions, the embedment depth in saturated sand was larger than in unsaturated sand.

Liu et al. (2012a) showed a theoretical framework for predicting the trajectory of drag embedment anchors based on a kinematic model and mathematical derivations. In this paper, a kinematic model and a theoretical framework for drag anchors in idealized and real states for predicting the trajectory was established. To examine the sensitivity, effectiveness and accuracy of the kinematic model and theoretical framework, parametric and comparative studies were preformed. The kinematic model in an

idealized state is the basis for establishing the kinematic model in a real state (Figure 12).

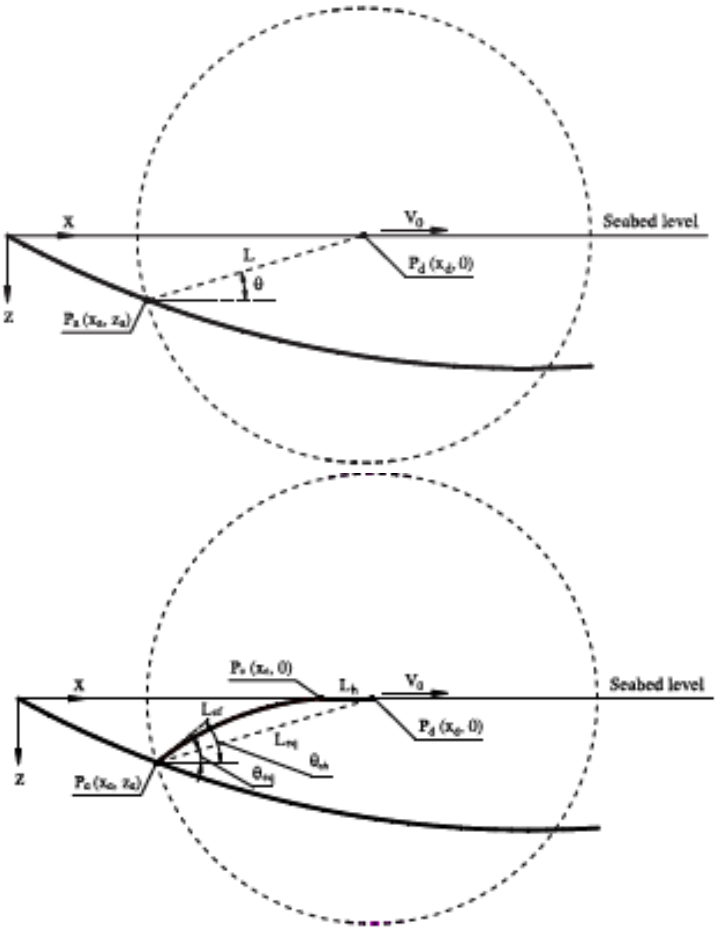

Figure 12. Kinematic model in an idealized state (first) and in a real state (second). (adapted from Liu et al., 2012a).

This work showed that the length and the drag angle at the shackle influences the drag curve significantly. In order to exactly predict the trajectory of drag anchors, the drag angle at the shackle has to be determined. The authors showed that the anchor

behavior in soils can be completely described by a theoretical model and mathematical Equations.

Liu et al. (2012b) discussed the movement direction of drag embedment anchors. This study showed an analytical method for predicting the movement direction of the drag anchor with an arbitrary fluke section. The method is based on a rational mechanical model for drag anchors and the knowledge of the mechanism that the anchor penetrates and moves in sand and clay.

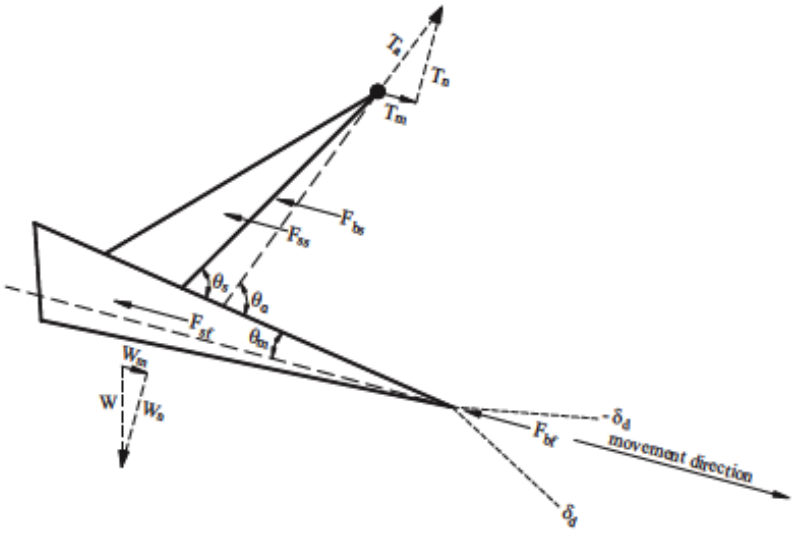

Figure 13. Mechanical model of a drag anchor and its movement direction (adapted from Liu et al., 2012b).

Two models are discussed in this paper: the theoretical model (rational mechanical model) and the analytical model to predict the movement direction. Clear prediction results are obtained then for an anchor with a rectangular and a wedge shaped fluke.

The experimental data are compared with the theoretical predictions and the agreement is satisfactory. The present work demonstrated that the movement direction of the anchor with an arbitrary fluke section could be reasonably determined by the developed analytical method. The study proved that the stable movement direction of the rectangular anchor is along the fluke surfaces (top or bottom surfaces). The unstable movement of the wedge anchors is along the top surface and the stable movement is along the bottom surface of the fluke. The behavior of these anchors in soil can be understood just by determining the movement direction of the anchors. Also the mooring line or dragline profile is important to precise the trajectory. To improve the drag embedment performance, precisely predicting the anchor trajectory, and solving the positioning problem it is important to understand and describe reverse catenary properties of the embedment line (Figure 14). The dragline of drag embedment anchors can be identified in three segments during movement of the anchor handling vessel (AHV) and penetration of the anchor. The top segment in the water is called catenary line, which takes on a catenary shape due to the self-weight of steel chains. The middle segment on the seabed called the horizontal line, which lies on the seabed and the bottom segment below the seabed called the embedded line (takes a reverse curvature compared with the catenary line in the water) (Liu et al., 2012a).

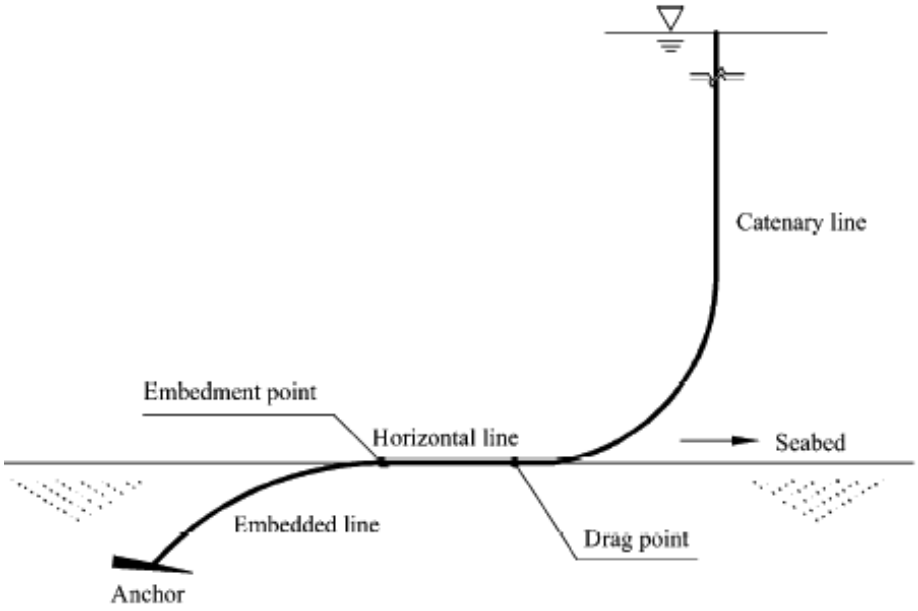

Figure 14. Definition of the dragline and its shape during penetration (adapted from Liu et al., 2012a).

from the University of Texas published a report about the initiation of movement for drag embedment anchor (Figure 15) and vertically loaded anchor models (Figure 16). Initial embedment stages of the anchor models are summarized in that report.

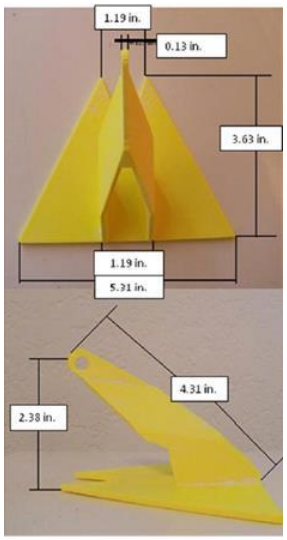

Figure 15. Drag embedment anchor model, DEA (adapted from Gilbert et al., 2013).

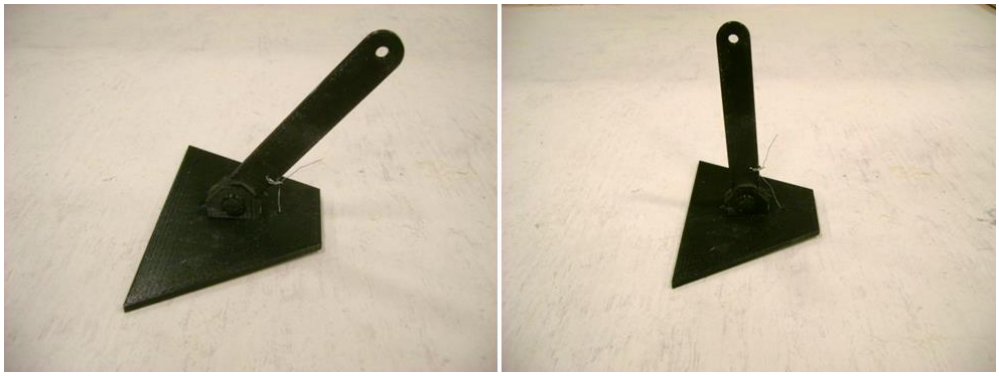

Figure 16. Vertically loaded plate anchor model, VLA (adapted from Gilbert et al., 2013).

By performing experimental tests on the anchors under pure loading, the behavior of both anchors at the initial embedment stage was observed. The tests were performed in normally consolidated kaolinite. After that, the force equilibrium diagram of various

anchor orientation in the initial embedment stage were analyzed and calculated. Figure 17 shows the various orientation modes, which were analyzed, where case 1 and 2 are DEAs and the other cases VLAs.

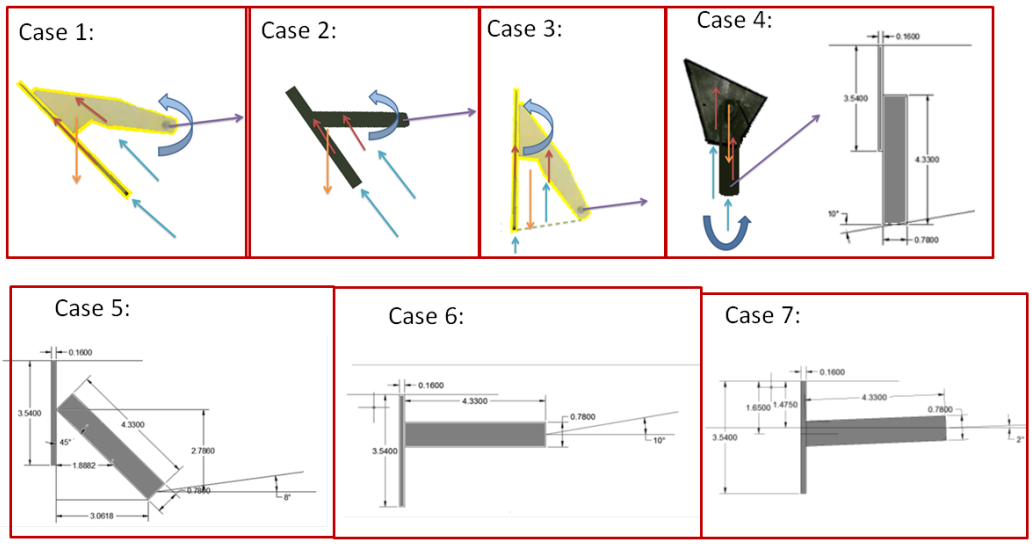

Figure 17. Graphical representation of analyzed orientation cases (adapted from Gilbert et al., 2013).

Therefore the total resistance under in-plane shear loading, normal loading and moment loading is calculated. The utilization ratio U.R. for each loading condition could be determined by comparing the line load and the bearing capacity. Equation 5 shows the U.R. for forces.

$$\text{U.R.}\,(\%) = \frac{S_u A N_c}{F} 100 \tag{5}$$

where S_u is the undrained shear strength, A is the bearing area, N_c is the bearing

capacity coefficient, and F is the line load. The U.R for moment is calculated with Equation 6.

$$\text{U. R. } (\%) = \frac{S_u A_f N_m L}{M} 100 \tag{6}$$

where A_f is the fluke area, N_m is the bearing factor for pure rotation, L is the length of the fluke (assumed the anchor is an equivalent square), and M is the moment.

The utilization ratio was calculated to define initial mode of failure and were compared with the experimental observations to check the accuracy of the calculation. The highest utilization ratio between in-plane shear, normal, and moment loading shows the mode that fails first and consequently the direction of movement of the anchor. The authors found out that the VLA will start to fail in-plane shear direction when the anchor fluke has an angle of 20 to 25 degrees with an anchor-line force angle of 0 to 5 degrees. It moves parallel to its fluke if the angle is 0 to 45 degrees from horizontal. The fluke-shank angle has no significant effect unless the shank opens up higher than 90 degrees and pulls the anchor out. Huang (2015) presented the same investigation for Flying Wing Anchors.

2.2 SYNTHESIS

The literature review indicated that there were no studies that have looked into the kinematics of plate anchors in sand that are initially embedded (e.g., through dynamic penetration), so all anchors in the studies assume that the anchor starts at the seabed. The literature also showed that the static capacity at various failure modes and the ultimate embedment depth are important aspects of a kinematics analysis. Also the shape of the anchor plays an important part. Both 1g model testing, performed by Liu et al. (2010a), and centrifuge modeling, performed by Neubecker and Randolph (1996), have been used to study anchor kinematics in the laboratory. The report from Gilbert et al. (2013) and Huang (2015) shows also an analytical model that uses bearing factors to calculate failure forces during various orientations, which are compared with the applied forces to estimate utilization ratios. This model can also be used in sand to estimate the complete trajectory. The Equations 5 and 6 have to be changed for sand cases:

$$\text{U. R. } (\%) = \frac{\sigma'_v A N_\gamma}{F} 100 \tag{7}$$

where σ'_v is the vertical effective stress, A is the bearing area, N_γ is the bearing factor, and F is the line load.

$$\text{U. R. } (\%) = \frac{\sigma'_v A_f N_\gamma L}{M} 100 \tag{8}$$

where A_f is the fluke area, L is the length of the fluke (assumed the anchor is an equivalent square), and M is the moment.

Using Equations 7 and 8 the utilization ratios for some finite displacement or penetration modes can be determined by using the bearing factors, which will be determined in this thesis. The anchor will take the path of least resistance, which is the force with the highest utilization ratio.

CHAPTER 3: 1g SMALL-SCALE TESTING METHODOLOGY

This chapter describes the methods used to perform 1g model tests on the Flying Wing Anchor under pure loading. Pure loading is regarded to be a single force acting on the anchor, such as pull, push or moment forces. This includes the test facility, test soil, soil preparation, and test set-up and procedures.

3.1 PURE LOADING MODES

The physical model testing will be performed on the Flying Wing Anchor under various modes of pure loading. The pure loading conditions were described in Chapter 1 and illustrated in Figure 3. The actual anchor trajectory would utilize certain combinations of these pure loading conditions along its entire path.

3.2 TEST TANK

The Anchor tests were performed in a 1g-test tank that was developed for 1:20 scale testing as shown in Figure 18. The tank was constructed to test shallow anchors in a controlled environment in the Geotech Laboratory in Bliss Hall at the URI Kingston campus. It is considered to be shallow, because an embedment depth over anchor fluke length (H/B) was less than 5. The test tank had inside dimensions of 914 mm height, 2413 mm length and 1219 mm width. For the bottom and the sidewalls, plywood was used and was reinforced with wooden beams. Two identical tanks have been constructed. Only one has been used for testing, where the other tank was used as a storage tank for the sand. The tanks were constructed already for a previous study on the capacity of anchors (Dietrich, 2014).

Figure 18. Photograph of the 1g-test tank (right) and the storage tank (left) at URI.

3.3 TEST SOIL

The sand, which was used for the tests, is a quartz beach sand from Westerly, Rhode Island. Several laboratory tests were performed to characterize the sand, including grain size, isotropically consolidated drained triaxial compression tests and determination of the critical state friction angle. Joseph Giampa at URI performed the testing and the results are presented here in a summarized form.

The sand is a fairly uniform gradation with grain sizes from 0.2 to 1 mm and no fines. It is poorly graded sand, according to the United Soil Classification System (ASTM D 2488-00).

Table 1. Soil properties of the Rhode Island beach sand used in this thesis.

γ_{max} (kN/m^3)	18.1
γ_{min} (kN/m^3)	14.1
e_{max}	0.844
e_{min}	0.436
ϕ_{cs} (deg)	33.4
D_{10} (mm)	0.19
D_{30} (mm)	0.27
D_{50} (mm)	0.30
D_{60} (mm)	0.31
C_u	1.63
C_c	1.24

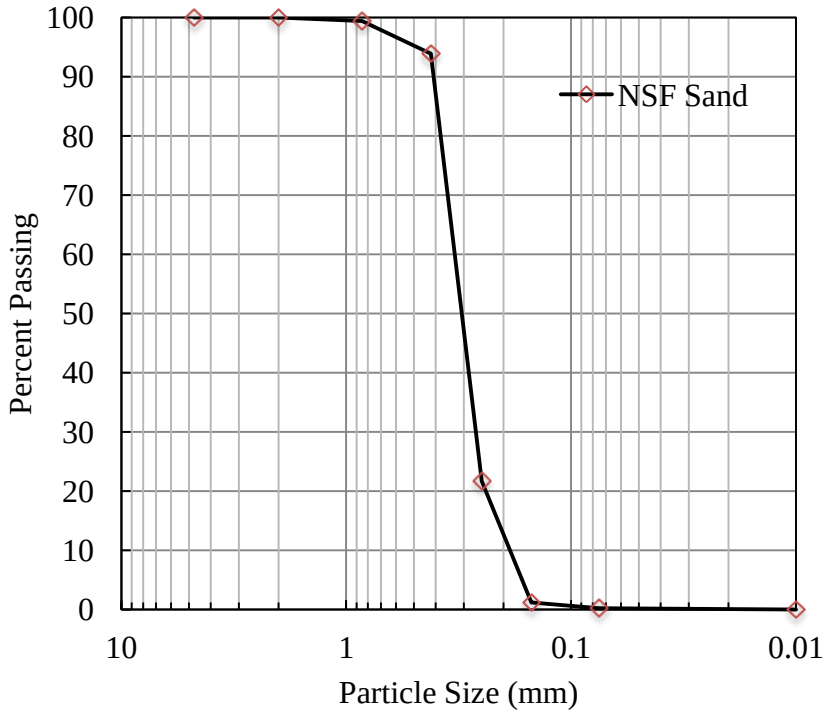

Figure 19. Sand particle size distribution.

3.4 SOIL PREPARATION

The soil placed in the test tank using pluviation equipment and procedures outlined in Dietrich (2014). As the effective confining pressure in a soil decreases the tendency for dilation will increase. Therefore, a 1g model will have similar constitutive response (i.e., strength and dilation) as the full-scale prototype if it is prepared looser. Dietrich (2014) prepared the soil to 20% relative density (very loose) to achieve a loose sand (~35% relative density) at the prototype scale.

The soil was air pluviated into the tank using a portable system similar to the one proposed by Gade et al. (2013) as shown in Figure 20. The pluviator is composed by a bucket, were the sand was dumped in, and a tube with two sieves allows the sand to be placed into the tank. The pluviator was attached to an overhead mobile gantry (Figure 21) and were controlled through an electric cable winch (Figure 22) allowing it to be adjusted laterally and vertically. The electric winch was placed and stabilized with weights on the floor. The steel cable from the winch was connected to a pulley system on the gantry.

Figure 20. Photograph of the portable pluviator developed by Giampa (2014) and Dietrich (2014) and adapted from Gade et al. (2013).

Figure 21. Photograph of the overhead mobile crane above the test tank.

Figure 22. Photograph of the electric steel cable winch.

The unit weight of the soil was measured during soil placement. Six identical cups were placed at the corners and middle of the tank (Figure 24). Measurements were made every 50.8 to 101.6 mm (4 to 2 in) layer of sand that was placed in the tank. The unit weight γ' inside the caps was calculated by dividing the measured weight of the soil inside the cup from the known inside volume of the cup. Relative density (D_r) was calculated from the following:

$$\mathrm{Dr} = \frac{\gamma' - \gamma' \mathrm{min}}{\gamma' \mathrm{max} - \gamma' \mathrm{min}} \frac{\gamma' \mathrm{max}}{\gamma'} \tag{9}$$

The test from the first horizontal normal fluke test shows an example for the density readings (Figure 23). The average unit weight for all tests could be determined as 14.69 to 14.8 KN/m^3. All tests provided an average relative density of 18 to 21%.

Table 2. Average density cups reading for each test.

Test # (-)	Dr Average (%)	Unit weight γ' Average (KN/m^3)
1	0.20	14.74
2	0.19	14.71
3	0.21	14.79
4	0.21	14.78
5	0.18	14.71
6	0.21	14.79
7	0.20	14.75
8	0.20	14.75
9	0.19	14.71
10	0.18	14.69
11	0.19	14.74
12	0.19	14.71
13	0.21	14.80
14	0.21	14.78
Average	0.20	14.75

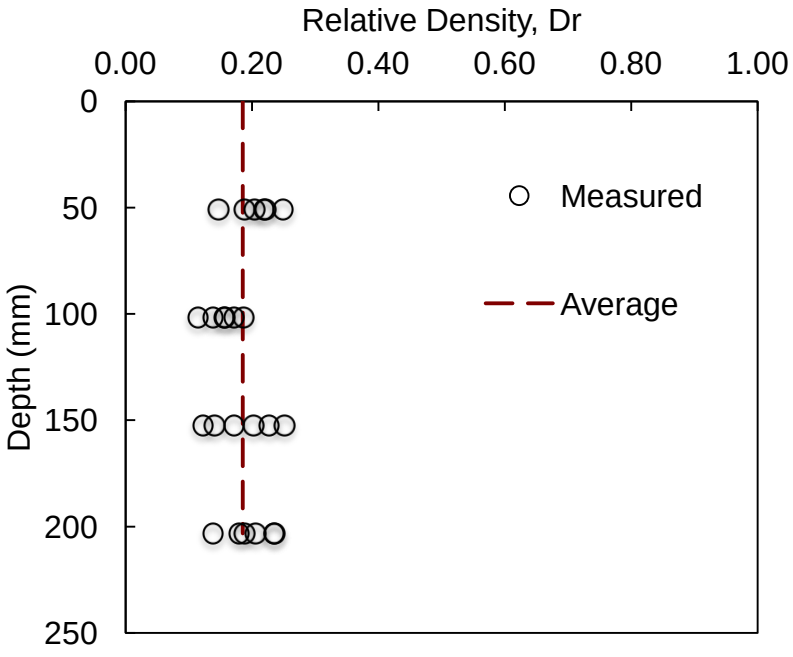

Figure 23. Density cups reading for the first in-plane shear (horizontal fluke) test.

Figure 24. Photograph of density cups readings during normal (vertical fluke) test.

3.5 IN-PLANE SHEAR (VERTICAL FLUKE) TESTS

This section describes the in-plane shear (vertical fluke) tests that were performed both in the downward and upward directions. Four anchor tests were performed in the first tank and three tests in the second.

3.5.1 MODEL ANCHOR

The model anchor has a base of 127 mm (5 in) and a height=B of 105.918 mm (4.17 in) for the in-plane shear (vertical fluke) tests. The thickness of the anchor is 12.7 mm (0.5 in). It is fabricated by steel and a rod was attached to the tip (Figure 26). The rod should provide a smooth and controlled penetration to the soil. The steel rod with a diameter of 9.525 mm (3/8 in) and a length of 482.6 mm (19 in) was welded on the back of the small anchor. The thickness of the rod was designed to prevent buckling (Hibbler, 2008). The anchor with the rod weighs about 0.989 kg (2.185 lbs = 9.719 N).

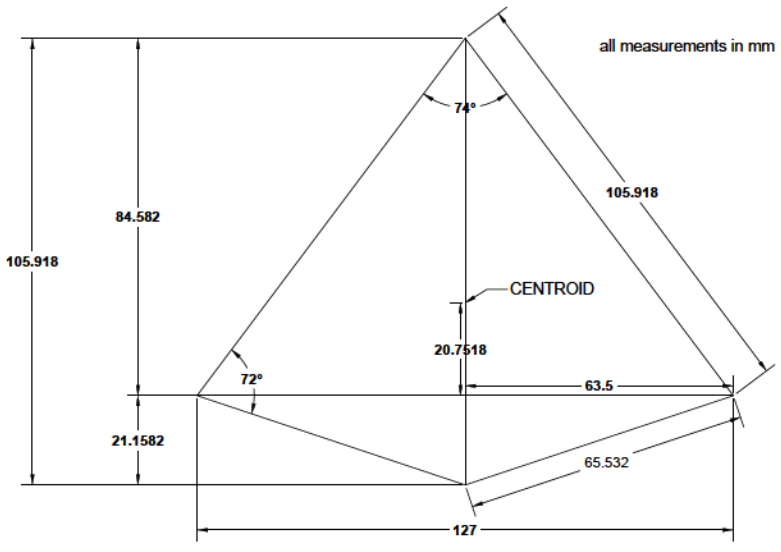

Figure 25. Anchor model dimensions for in-plane shear (vertical fluke) tests.

Figure 26. Photograph of the anchor model with attached rod.

3.5.2 TEST SET-UP

The anchor was pushed into the soil bed using the system shown in Figure 27. To provide enough weight to move the anchor into the soil, 3 weight plates were used. The orange plate (seen on Figure 28) has a weight of about 32.2026 Kg (315.8 N=71 lbs) and the two black plates (Figure 27) with a weight of about 22.678 kg (222.4 N=50 lbs). The weight ensures that the anchor penetrates the soil. The orange plate was not removed after the push test, while the other two lighter weights were removed after penetration. The electric winch could pull the anchor with the orange weight on it.

Figure 27. Photograph of the test anchor for the in-plane shear (vertical fluke) test with all weights.

Figure 28. Photograph of the test anchor for the in-plane shear (vertical fluke) with reduce weight.

The anchor was pushed and pulled into the soil in certain places to minimize boundary effects. The load cell from CAS was attached between the weights and the rod of the anchor. A 2224 N (500 lbs) capacity load cell was used for all the push and pull tests. A smaller capacity load cell was chosen to measure loads at higher precision (Figure 29).

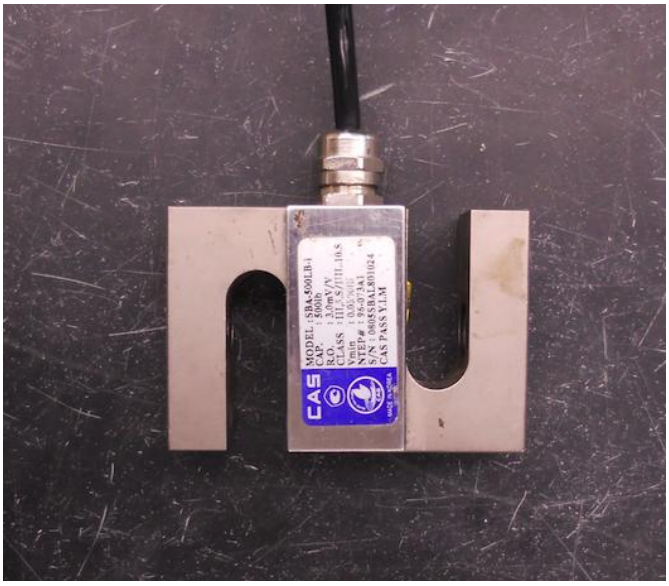

Figure 29. Photograph of the load cell.

The anchor with the weights was attached to a block-and-tackle system, which went through a pulley on the mobile gantry and was fixed on a steel cable that was provided by the electric winch. The string potentiometer, which was connected to the anchor and located at the mobile gantry, was used to measure the displacements of the anchor in the soil (Figure 30). The string potentiometer measured the displacement in inches.

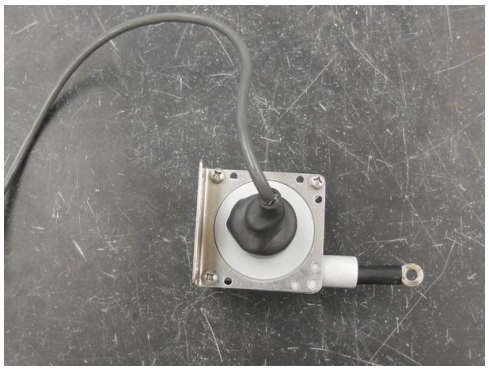

Figure 30. Photograph of the string potentiometer with a total length of 1270 mm (50 in).

The load cell and the string potentiometer were connected to the data acquisition system (Figure 31 and Figure 32). The acquisition system was connected to a laptop. To record the tests a power supply with a data acquisition system manufactured by i100 instruNet was used, which was connected to the laptop.

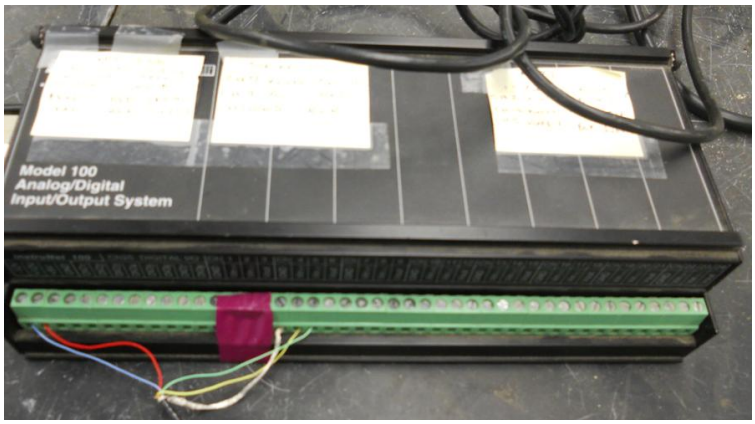

Figure 31. Photograph of the i100 instruNet acquisition system for load cells, torque sensor and string-pot.

Figure 32. Photograph of the power supply.

3.5.3 TEST PROCEDURE

For the push (downward) test the anchor hung initially approximately 6.35 mm (1/4 in) above the sand bed surface. The orange weight was mounted to the steel rod outside of the test tank. Two weights were attached to the orange weight while it hung above the seabed of the test tank. The anchor took a vertical position with the tip facing the tank (Figure 27). The electric winch controlled the rope-steel cable system. By easing the steel cable controlled with the electric cable winch, the anchor penetrated the soil at a constant rate of 5 cm/s. The steel cable was attached to a pulley system to provide controlled vertical push and pull movements of the anchor. The anchor with weights had to be slightly guided in manually; otherwise the anchor with rod would tilt to the side. Although the anchor was continuously pushed into the soil, it was attempted to get bearing factors at specific depths with this method.

The measured load therefore represents the total resistance (bearing and side friction) of the anchor during penetration. To account for the anchor weight and rod weight, the downward load readings were zeroed during post processing, i.e. the baseline of the measured load was shift to zero when processing the data.

After pushing the anchor, the same anchor was pulled vertically upwards. Therefore the two lighter weights were removed from the rod, while the orange plate was still attached. The electric winch was used to pull the anchors vertically through the soil with a constant rate of 5 cm/s. During the pull test no manual guiding was necessary.

The weight of the anchor and the rod had to be subtracted when processing the data. The orange plate is above the load cell and does not affect the measurement.

3.6 NORMAL (VERTICAL FLUKE) TESTS

Three normal (vertical fluke) tests were performed as described below.

3.6.1 MODEL ANCHOR

The model anchor has a base of 236.22 mm (9.3 in) and a height of 196.85 mm (7.75 in) for the normal (vertical fluke) tests. The thickness of the anchor is 12.7 mm (0.5 in). It is made of steel (Figure 34). A padeye was attached at the area centroid of the anchor, so the anchor could be pulled horizontally without tilting movements while it lies vertically in the sand. The anchor weighs about 2.404 kg (5.3 lbs = 23.58 N).

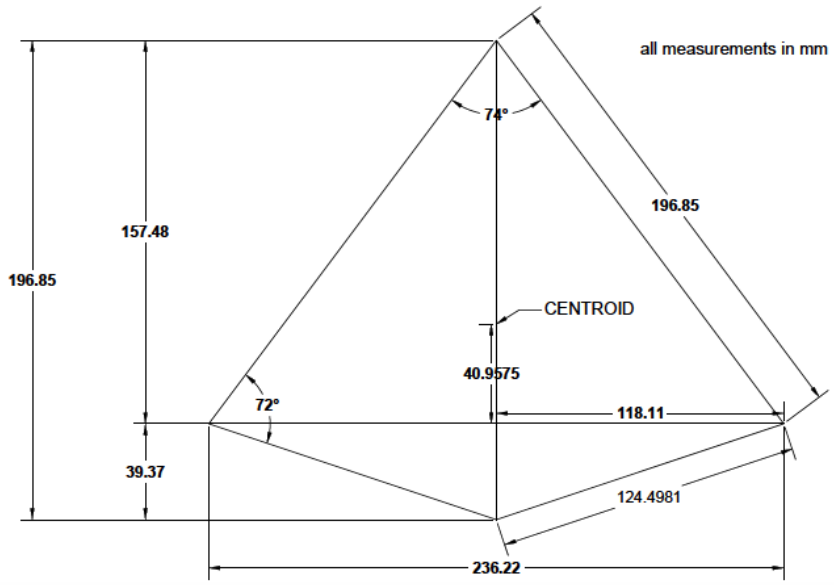

Figure 33. Anchor model dimensions for the normal (vertical fluke) and in-plane shear (horizontal fluke) tests.

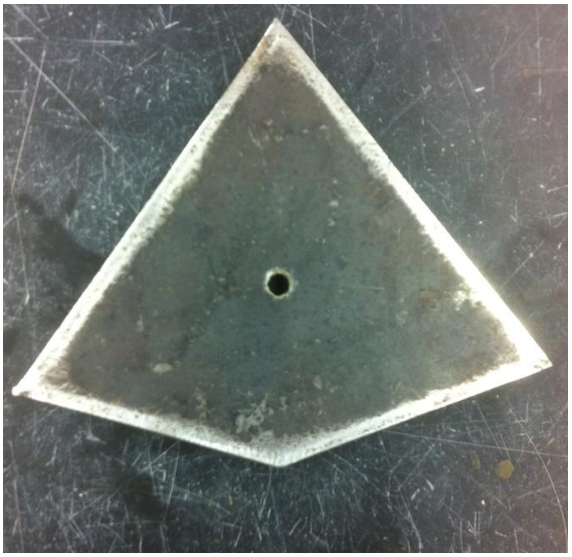

Figure 34. Photograph of the anchor model with padeye in the centroid for the normal (vertical fluke) tests.

3.6.2 TEST SET-UP

To provide the maximum drag displacement through the tank only one anchor could be tested. One test was a repeat test to prove the reliability of the measured data. For all tests the anchor was laid vertically on a 203.2 mm (8 in) thick sand layer (Figure 35). To provide no rotational movement of the anchor during the drag, a steel string was fixed on steel ring, which was screwed into the area centroid of the anchor. The anchor was placed 127 mm (5 in) from the back wall in the center of the box.

The steel string was connected to the pulley on the inside front wall and was attached to the load cell. The pulleys have a bearing inside; thereby no friction could increase the resistance during the tests. One pulley was attached on the gantry and another pulley on the front wall inside the box. Steel cables were used to pull the anchors. The load cell was fixed to the ropes. The ropes went through a pulley on the gantry and were attached to the electric cable winch. The string potentiometer (Figure 30) was attached to a hook between load cell and the ropes attachment (Figure 29). A 2224 N (500 lbs) and 11121 N (2500 lbs) capacity load cell from Omega were used for the tests, because it was assumed that at an embedment ratio bigger or equal to H/B=2, the resistance or load will exceed the 2224 N (500 lbs) (Figure 27).

The load cell and the string potentiometer were connected to the data acquisition system (Figure 31 and 32). The acquisition system was connected to a laptop.

For the first test, where the embedment depth was H/B=1, the tank was filled to 206.4 mm (16 in), so the anchor was embedded 203.2 mm (8 in). For this test the 2224 N (500 lbs) load cell was used. The same pluviation procedure was used for the tests as for the in-plane shear (vertical fluke) tests. For the second test, where the embedment depth was H/B=2, the tank was filled to 609.6 mm (24 in), so the anchor was embedded 206.4 mm (16 in). For this test the 11121 N (2500 lbs) load cell was used. The test with the embedment depth of H/B=1 was re-performed in order to prove the reliability of the measurements.

Figure 35. Photograph of the test anchor for the normal (vertical fluke) tests.

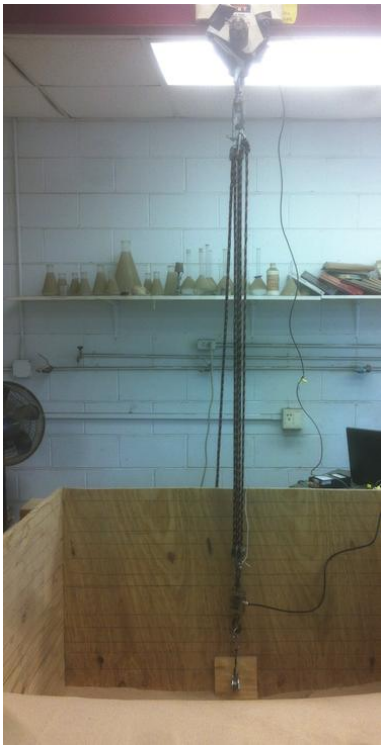

Figure 36. Photograph of the anchor attachment on the wall for the normal (vertical fluke) tests.

3.6.3 TEST PROCEDURE

The anchor was placed vertically in the soil and was pulled horizontally through the soil to maximize the distance between the anchor and the walls of the tank. The rope-steel cable system was pulled at a constant rate using the winch and the load cell and potentiometer were recorded. The weight of the anchor and rod had to be subtracted from the measured load readings during post processing.

3.7 PITCH ROTATION (VERTICAL FLUKE) TESTS

Three pitch rotation (vertical fluke) tests were performed.

3.7.1 MODEL ANCHOR

The anchor for the pitch rotation (vertical fluke) tests was fabricated from aluminum (Figure 37) so that a magnetic tracking device could be used to determine the rotation of the anchor during the test. The same dimensions as for the normal (vertical fluke) model anchor were taken. However, the anchor thickness was increased to 15.875 mm (5/8 in) to allow a recess to be constructed in the tail of the anchor to place a magnetic tracking sensor.

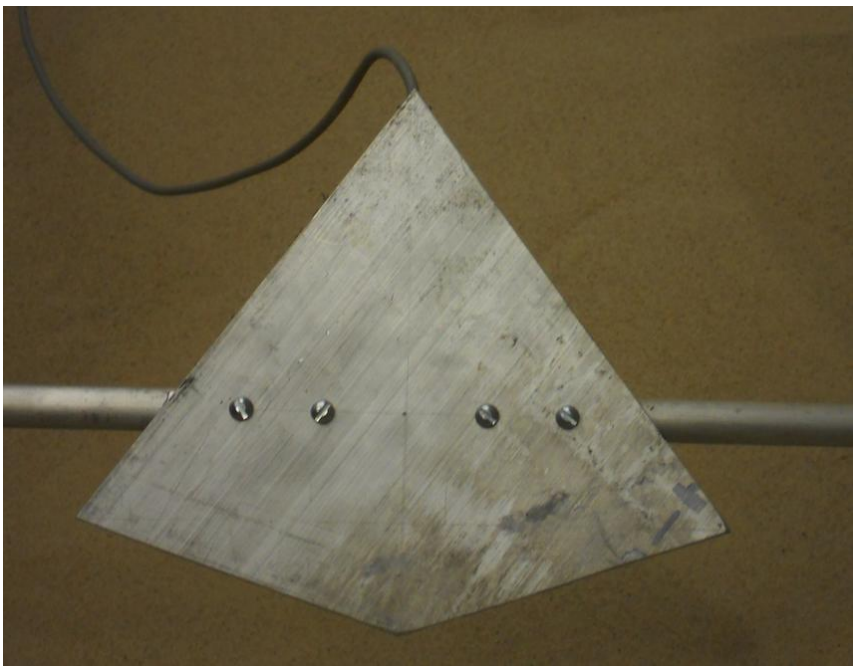

Figure 37. Large anchor model dimensions with rod attachment on the side and cut-out for the tracking device for the pitch rotation (vertical fluke) tests.

3.7.2 TEST SET-UP

To provide the maximum rotation of the anchor without boundary issues in the tank only one anchor could be tested within the tank. For all tests the anchor was positioned vertically on a 228.6 mm (9 in) thick sand layer (Figure 42).

For the moment tests an aluminum rod with a diameter of 15.875 mm (5/8 in) was attached to the aluminum anchor to allow it to be rotated (Figure 38). The rod was designed to accommodate the anticipated torque levels (Hibbler, 2008). A rod diameter of 15.875 mm (5/8 in) was used.

The anchor was attached to the rod at the area centroid of the anchor. The rod was flattened on the attaching part and was fixed with four aluminum screws. The rod was solid aluminum and had a length of 609.6 mm (24 in). On the back tip of the anchor an attachment point was cut out to attach the tracking device. The tracking device was fixed with silicon. The anchor weighs about 1.016 kg (2.2403 lbs = 9.965 N).

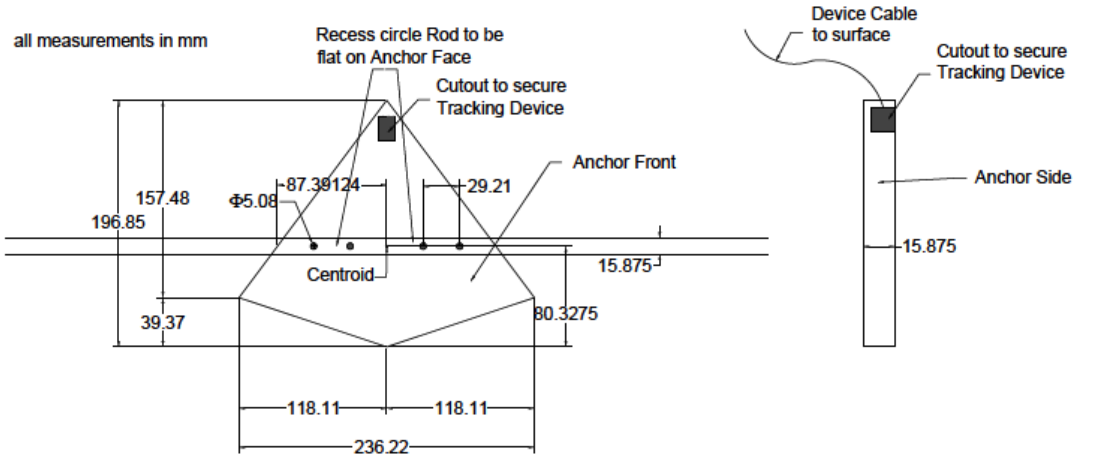

Figure 38. Large anchor model dimensions with rod attachment on the side and cut-out for the tracking device for pitch rotation (vertical fluke) tests.

Two holes were drilled through the sides of the tank walls to all the installation of the anchor rod. One side the rod was attached to a torque sensor (Figure 43 and Figure 44). Both holes were mounted with a ball-bearing flange, so that the rod with anchor could rotate smoothly and with minimal friction. On the torque sensor side the rod was attached to a lever arm made of aluminum, were the rotation could be performed manually (Figure 45). A torque sensor from Omega with 226 Nm (2000 lbs-in) capacity reading was used for the tests (Figure 39).

Figure 39. Photograph of the torque sensor.

A tracking device from Polhemus was used to measure the rotation angle of the anchor during testing. The system consists of a source (Figure 40), sensor, and system electronics unit (Figure 41). The electronics unit is interfaced with the laptop computer for displace and data acquisition.

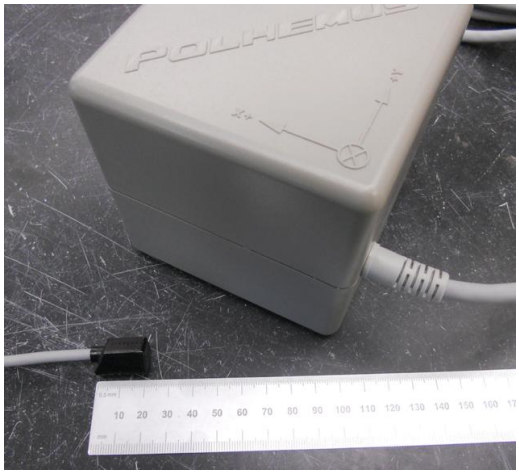

Figure 40. Photograph of the magnetic tracking device source.

Figure 41. Photograph of the Polhemus Patriot system electronics unit.

For the first test, where the embedment depth was H/B=1, the tank was filled to 431.8 mm (17 in), so the anchor was about 203.2 mm (8 in) embedded. The same pluviation procedure was used for the tests as for the other pure loading tests. For the second test, where the embedment depth was H/B=2, the tank was filled to 635 mm (25 in), so the anchor was about 406.4 mm (16 in) embedded. For the last test, where the embedment depth was H/B=3, the tank was filled to 838.2 mm (33 in), so the anchor was about 609.6 mm (24 in) embedded.

Figure 42. Photograph of the torque sensor dimensions outside the test tank.

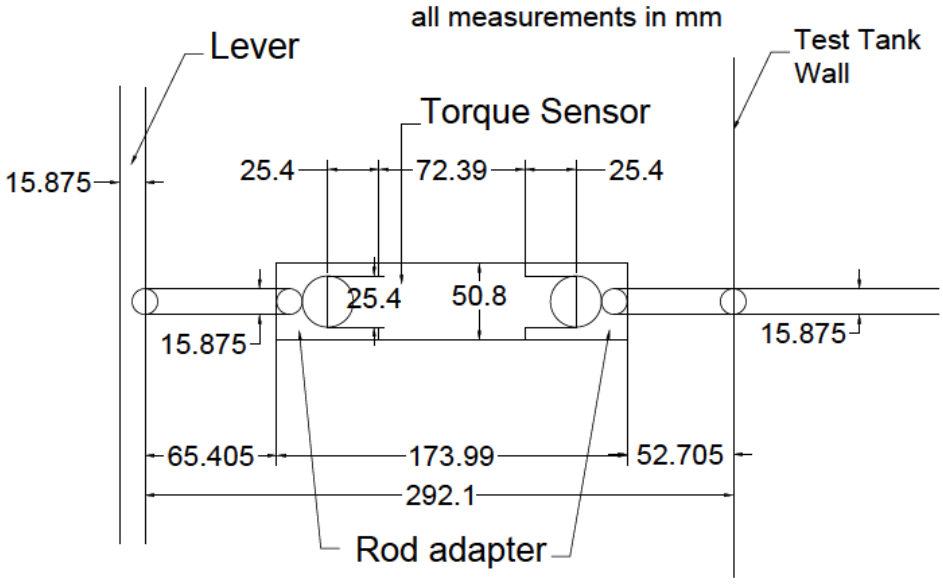

Figure 43. The torque sensor dimensions outside the test tank.

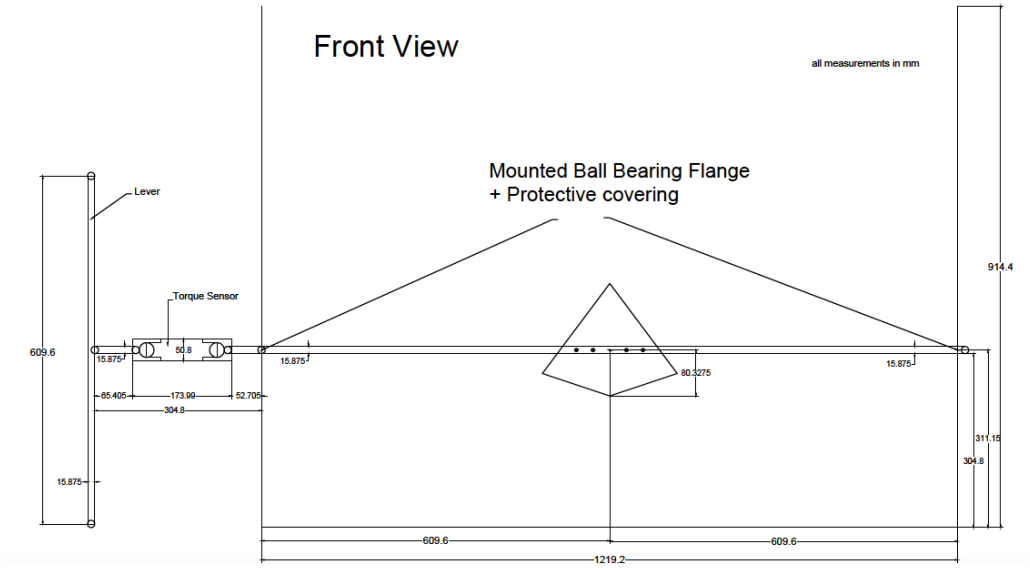

Figure 44. The front view test tank with dimensions for lever, anchor, and torque sensor for the pitch rotation (vertical fluke) tests.

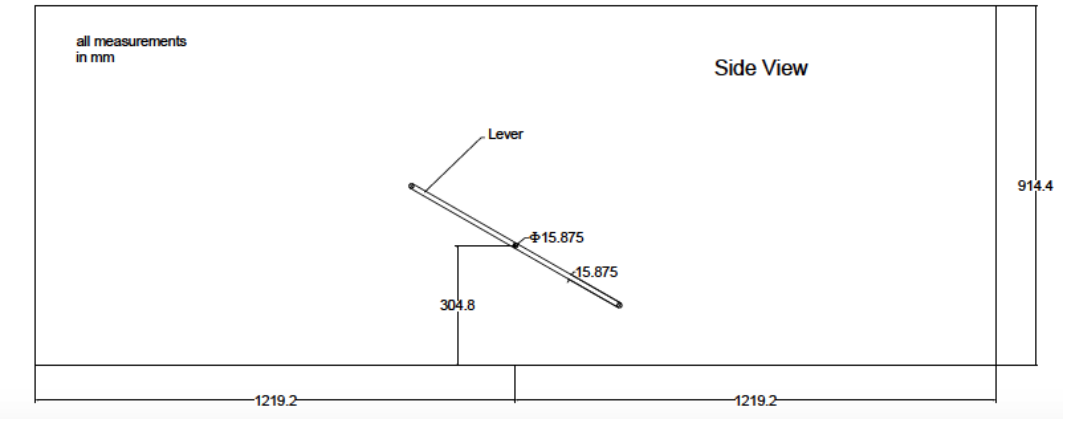

Figure 45. The side view test tank with dimensions for lever for the pitch rotation (vertical fluke) tests.

3.7.3 TEST PROCEDURE

The anchor was initially positioned in a vertical orientation and was then rotated in the soil. The lever arm was torqued manual with constant speed. The rod was rotated 180 degrees in all tests. Data from the torque sensor and magnetic tracking device were recorded during testing. Some tests were also performed with the anchor removed to measure the rod and bearing friction that were removed later during data processing.

3.8 IN-PLANE SHEAR (HORIZONTAL FLUKE) TESTS

Six in-plane shear (horizontal fluke) tests were performed.

3.8.1 MODEL ANCHOR

The same anchor, which was used for the normal (vertical fluke) tests, was also used for the in-plane shear (horizontal fluke) tests (Figure 33 and 34). The centroid thread was filled and a pad eye was attached to the tip of the anchor, so the anchor could be pulled exact horizontally while it lies horizontally in the sand bed.

3.8.2 TEST SET-UP

To maximize the space needed for lateral movement only one anchor was tested in a tank. For all tests the anchor was placed horizontally on a 203.2 mm (8 in) thick sand layer (Figure 46). The anchor was placed 127 mm (5 in) from the back wall in the center of the box.

A steel pad eye was screwed into the central point on the back tip of the anchor. A steel cable was then connected to that anchor that was fed through a pulley on the front wall of the tank and run vertically to the load cell and hoist system. The string potentiometer was attached to a hook between load cell and ropes (Figure 47). The test set-up is similar to the horizontal shear test ones. An 890 N (200 lbs), 2224 N (500 lbs) and 11121 N (2500 lbs) load cell (Figure 29) was used for the tests. The load cell

and the string potentiometer (Figure 30) were connected to the data acquisition system (Figure 31 and 32). The acquisition system was connected to a laptop.

For the first test, where the embedment depth was H/B=1, the tank was filled to 406.4 mm (16 in), so the anchor was at 203.2 mm (8 in) embedded. For this test the 890 N (200 lbs) load cell was used. The same pluviation procedure was used for the tests as for the in-plane shear (vertical fluke) tests. For the second test, where the embedment depth was H/B=2, the tank was filled to 609.6 mm (24 in), so the anchor was 406.4 mm (16 in) embedded. For this test the 2224 N (500 lbs) load cell was used. For the last test, where the embedment depth was H/B=3, the tank was filled to 812.8 mm (32 in), so the anchor was 609.6 mm (24 in) embedded. For this test the 11121 N (2500 lbs) load cell was used as well. All tests with the different H/B ratios were performed again, but for the second set the 2224 N (500 lbs) load cell were used, because it was notice that the load would not exceed 2224 N (500 lbs) for any of these test.

Figure 46. Photograph of the test anchor for the in-plane shear (horizontal fluke) tests.

Figure 47. Photograph of the anchor attachment on the wall for the in-plane shear (horizontal fluke) tests.

3.8.3 TEST PROCEDURE

The test procedure was similar to the normal (vertical fluke) tests.

CHAPTER 4: RESULTS AND DISCUSSION

This chapter will present the results of the experimental tests including calculations, results and discussion, and summary.

4.1 IN-PLANE SHEAR (VERTICAL FLUKE) DOWNWARD TESTS

This section presents the results of the in-plane shear (vertical fluke) downward tests.

4.1.1 CALCULATIONS

For the in-plane shear (vertical fluke) downward tests, the rod resistance (shear) was subtracted from the total resistance and also from the bearing factors, so that the resistance and other values could be determined only for the anchor.

The resistance was calculated by multiplying the calibration factor of the load cell with the load cell readings. The 2224 N (500 lbs) was used for the tests. The calibration factor for the 2224 N (500 lbs) load cell is 71.0 N/mV (15.97 lbs/mV) for the push tests. The calibration factors are negative during compression. The string potentiometer was measured in inches. The program i100 instruNet was used to read load and displacement data. As mentioned in section 3.5.3, the downward load readings were zeroed during post processing, i.e. the baseline of the measured load was shift to zero when processing the data, to account for the weight of the anchor and rod.

For each test a non-dimensional bearing factor N_γ were calculated. The bearing factors were calculated for the ultimate total resistance at failure (Q_{tu}), which combines shear and bearing, and the ultimate bearing resistance (Q_{bu}) at failure, which considers bearing resistance only. The bearing factors are empirical and are based on the bearing capacity theory for piles (Kulhawy and Mayne, 1990), which is:

$$q_u = cN_c + q'N_q + \gamma BN_\gamma \quad (10)$$

where c is cohesion of the soil, N_c is the cohesion coefficient, q' is the effective stress, N_q is the effective stress coefficient, γ is the unit weight, B is the pile diameter, and N_γ is the unit weight coefficient. Sand is mostly cohesion less, so c and N_c are zero, and B is small, so γ, B, and N_γ can be neglected as well. Follow Equation for sand can be then obtained:

$$q_u = q'N_q \quad (11)$$

The bearing resistance can be than calculated by:

$$R_t = q_u A_t = q'N_q A_t \quad (12)$$

and N_q is similar in concept to the bearing factor N_γ for this research. The bearing factor is further used to calculate the utilization ratio, which is needed for the analytical model that is explained in Chapter 2 (Gilbert et al., 2013 and Huang, 2015).

The N_γ for the in-plane shear (vertical fluke) downward tests were calculated by using Q_{tu} or Q_{bu} and H, and following Equations were used:

$$N_\gamma = \frac{Q_{tu}}{\gamma' H A_{fluke}} \tag{13}$$

$$N_\gamma = \frac{Q_{bu}}{\gamma' H A_{bearing}} \tag{14}$$

Where γ' is the effective unit weight of the soil, $A_{bearing}$ is the bearing area of the anchor, A_{fluke} is the fluke area of the anchor, and H is the embedment depth. The bearing factors (Equation 13) were calculated by using the fluke area to be consistent with the University of Texas (Gilbert et al. (2013) and Huang (2015)) and the bearing factors (Equation 14) were calculated by using the bearing area, which is consistent with bearing capacity theory (Kulhawy and Mayne, 1990). The $Q_t/\gamma' H A_{fluke}$ and $Q_b/\gamma' H A_{bearing}$ curves were calculated by using a variable Q and H. The vertical effective stress σ'_v ($\gamma' H$) has been used, because it is the easiest and most convenient confining stress to calculate.

In order to calculate the bearing factor, the area portions of the initial penetration have to be regarded in the bearing area. With increasing penetration depth the area increases till the complete fluke area is embedded.

To calculate the bearing percentage of the anchor, the shear force was estimated from

the following Equation:

$$Q_{shear} = \sigma'_n \tan(\delta) A_{shear} \quad (15)$$

where σ'_n is the horizontal effective stress or vertical effective stress (in this case it is the horizontal effective stress, because the anchor is vertically positioned), δ is the interface friction angle, and A_{shear} is the shear area. These values can be obtained with the following Equations:

$$\sigma'_v = \gamma' H \quad (16)$$

$$\sigma'_h = \sigma'_v K \quad (17)$$

$$K = 1.5(1 - \sin(\phi')) = 1.5K_0 \quad (18)$$

$$\delta = \frac{2}{3}\phi' \quad (19)$$

where K is the lateral earth pressure coefficient for soils. It will be multiply times 1.5 to account for an increase in the normal stress on the anchor due to soil displacement. The interface friction angle is assumed to be 2/3 of the effective peak friction angle, which is common for steel and sand interaction. The peak friction angle ϕ' was assumed to be 37 degrees based on triaxial test data (Giampa, Personal Communication).

By dividing the shear force Q_{shear} from the total force Q_t the percentage of the shear can be estimated and therefore also the bearing percentage. To estimate the rod shear resistance, the area of the rod was also included in Equation 15 to get the total shear percentage. After that, the actual shear force without the rod could be determined with Equation 20, by dividing the total shear area from the rod shear area (Equation 21).

$$Q_{shear} = Shear_{\%} Q_t \left(1 - \left(\frac{A_{shear}}{A_{rod-shear}}\right)\right) \quad (20)$$

$$A_{rod-shear} = \pi d_{rod} H \quad (21)$$

where d_{rod} is the rod diameter and $Shear_{\%}$ is the total shear percentage (with rod). By adding the new calculated shear resistance (without the rod resistance) to the bearing force, which was calculated with the bearing percentage, the actual Q_t without the rod can be presented. Based on the actual Q_t, the bearing factors were calculated by using Q_{tu} and Q_{bu}.

The fluke area for the bearing factors (Equation 13) and the bearing area for the bearing factors (Equation 14) were calculated as following:

$$A_{fluke} = \frac{pq}{2} \quad (22)$$

$$A_{anchor-bearing} = a d_{anchor} 2 \quad (23)$$

where p is the horizontal diagonal, q is the vertical diagonal, a is the bottom side length of the anchor, and d_{anchor} is the thickness of the anchor.

4.1.2 RESULTS

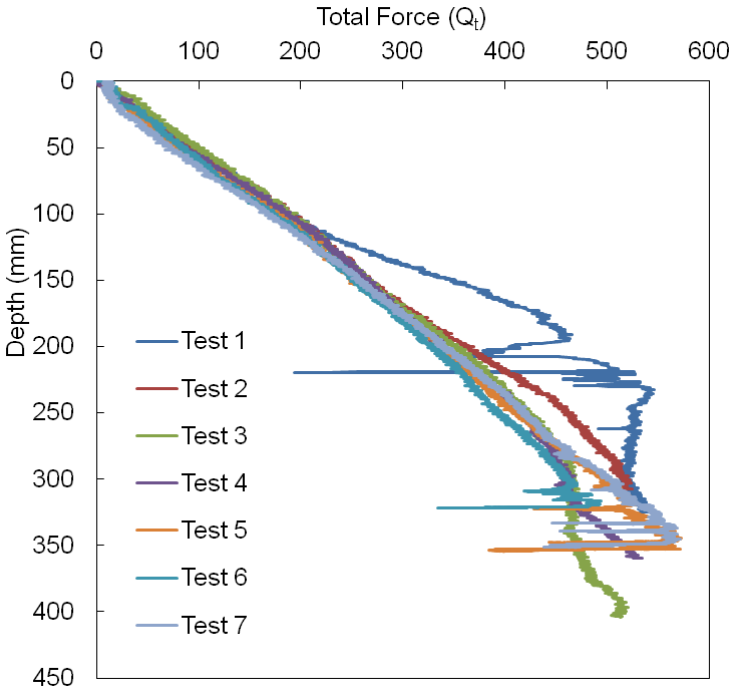

Figure 48. Results of the in-plane shear (vertical fluke) downward tests.

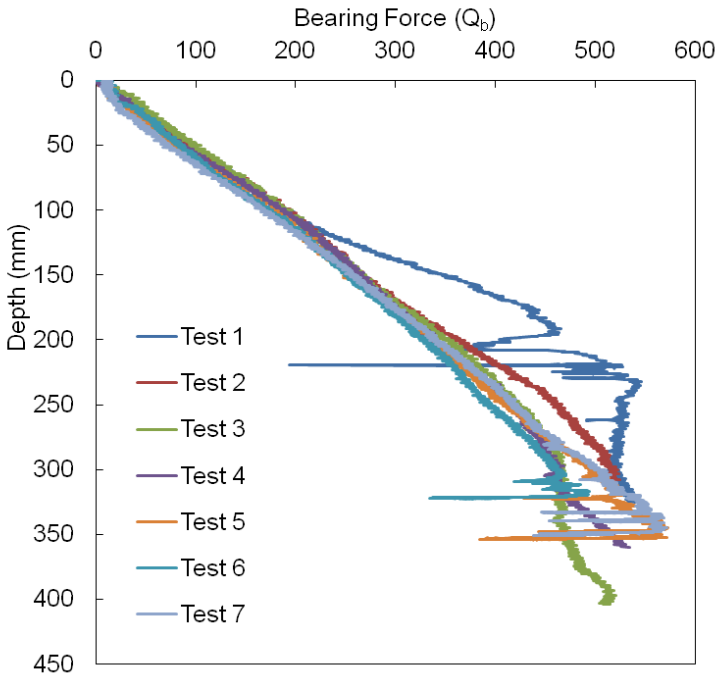

Figure 49. Results of the in-plane shear (vertical fluke) downward tests.

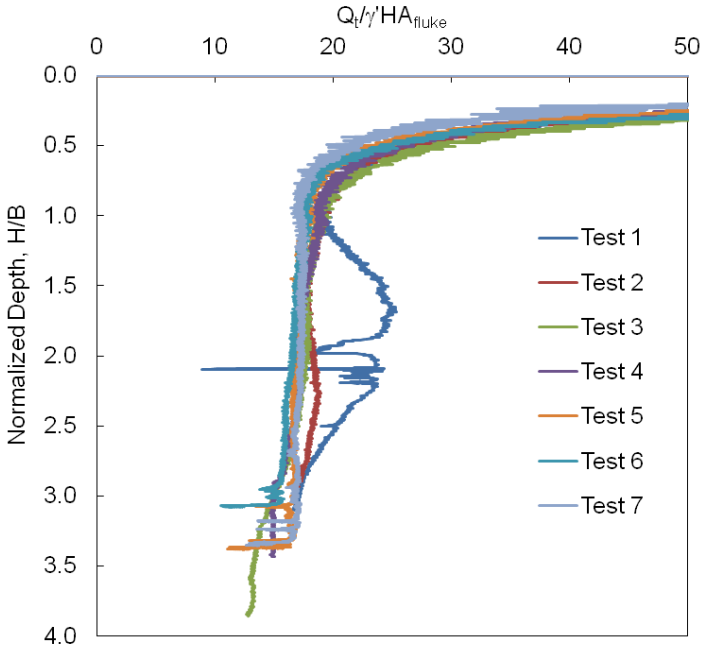

Figure 50. Normalized results of the in-plane shear (vertical fluke) downward.

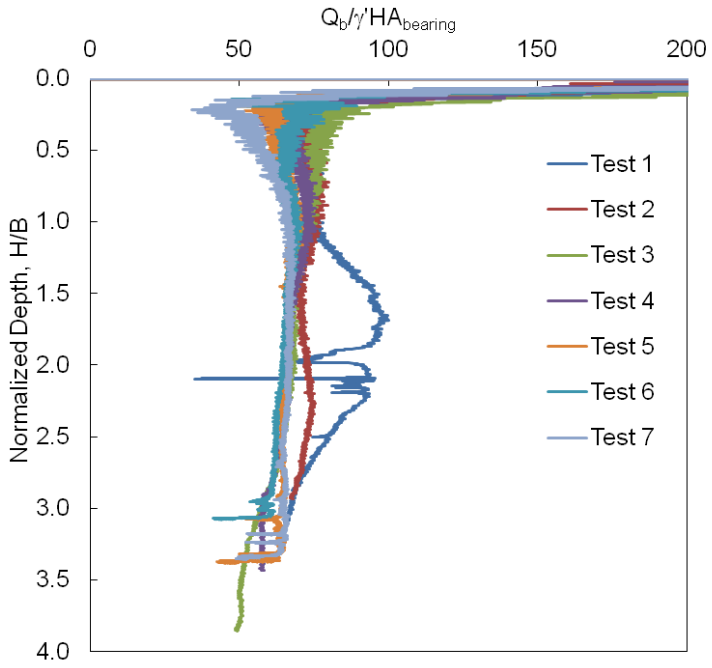

Figure 51. Normalized results of the in-plane shear (vertical fluke) downward.

Table 3. Summary of the bearing factors (Equation 13) for in-plane shear (vertical fluke) downward tests.

Test	2	3	4	5	6	7	Average
H/B=1	18.6	19	18.3	18.3	18.2	17.5	18.3
H/B=2	18.3	17.6	17.4	17.1	16.5	17.5	17.4
H/B=3	-	14.9	14.8	16.8	15.5	16.6	15.7

4.1.3 DISCUSSION

As shown in Figures 48 and 49, the resistances measured in tests 2 through 7 are all in the same range, i.e. the trends are similar. However, the first test shows a bump in the curve, which is caused by a lateral tilt during the test, and therefore this test was not included in the bearing factor calculations. The resistance increases with increasing depth.

The normalized resistance curves (Figure 50 and 51) are almost constant with depth below an embedment ratio of about 1. The initial high values of the bearing factors are caused by a small bearing and fluke area in combination with very low vertical effective stresses near the soil surface. This resulted in a high variability of the bearing factor at very shallow penetration.

The bearing factors (Equation 13) range from 16 to 18 and therefore appear to be relatively independent of the embedment depth. It is important to note, that the anchor was continuously pushed so the calculated resistance represents a fully mobilized resistance value. If the anchor had been placed to a specified embedment depth first and then loaded, the anchor would have to deform some amount to reach the peak resistance.

The resistance of the anchor is primarily from end bearing resistance at the tip of the anchor. Considering the bearing area has a width (i.e. plate thickness) that is much smaller than the embedment depth, it is likely that the failure mechanism is deep, in

other words the soil is failing locally around the tip of the anchor. The resistance is therefore being controlled by the shear strength of the soil near the tip, which should increase approximately linearly with embedment depth. Therefore, the normalization is accounting for the increase in overburden stress leading to constant bearing factors.

4.2 IN-PLANE SHEAR (VERTICAL FLUKE) UPWARD TEST

This section presents the results of the in-plane (vertical fluke) upward tests.

4.2.1 CALCULATIONS

For the tests, the rod resistance (shear) was subtracted from total resistance and from the bearing factors as well similar to the downward tests.

The resistance or capacity was calculated by multiplying the calibration factor of the load cell with the load cell readings. The 2224 N (500 lbs) was used for the tests. The calibration factor for the 2224 N (500 lbs) load cell is 70.32 N/mV (15.81 lbs/mV) for pull out tests. The calibration factors are positive during uplift. The capacity of the vertical upward test had to be adjusted because of the weight of the anchor and the rod. During pull it provides a compression force, i.e. the weight of the anchor acts against the pull and therefore against the load cell. By subtracting the weight of the anchor and the rod from the resulting capacity, the real pullout capacity can be determined. The weight of the plate above the load cell seen on Figure 28 does not affect the results, because when it hangs with the plate in the air it could be observed that the load cell reads zero. The anchor and the rod have a total weight of about 0.989 kg (2.185 lbs). That means 9.7194 N have to be subtracted from the capacities. The adjustment has been done for all tests and presented curves during post processing. The string potentiometer was measured in inches. The program i100 instruNet was

used to read load and displacement data.

For each test a non-dimensional bearing factor were calculated as well. The bearing factors were calculated with Equation 13 and 14 similar to the in-plane shear (vertical fluke) downward tests. For the in-plane shear (vertical fluke) upward test, the $Q_t/\gamma'HA_{fluke}$ and $Q_b/\gamma'HA_{bearing}$ curves were estimated with a fixed embedment depth H and the variable Q. A fix embedment was assumed to observe the bearing factor for the max resistance at the deepest embedment depth, which is based on White et al. (2008). He estimated the pull bearing factors for the uplift resistance of plate anchors in sand by using this approach.

To calculate the bearing percentage of the anchor and to get the total resistance without the rod resistance, the same procedure as for the in-plane shear (vertical fluke) downward test has been performed by using Equations 15 through 20. It showed that the shear percentage for the anchor is higher during upward than for the downward tests.

With the actual Q_{tu} (without rod resistance) and the Q_{bu}, which were obtained by the above-explained procedure, the bearing factors can be determined. The fluke area for the bearing factors (Equation 13) was calculated with Equation 22 and the bearing area for the bearing factor (Equation 14) was calculated as following:

$$A_{bearing} = bd_{anchor}2 \quad (24)$$

where b is the bottom side length of the anchor, and d_{anchor} is the thickness of the anchor.

4.2.2 RESULTS

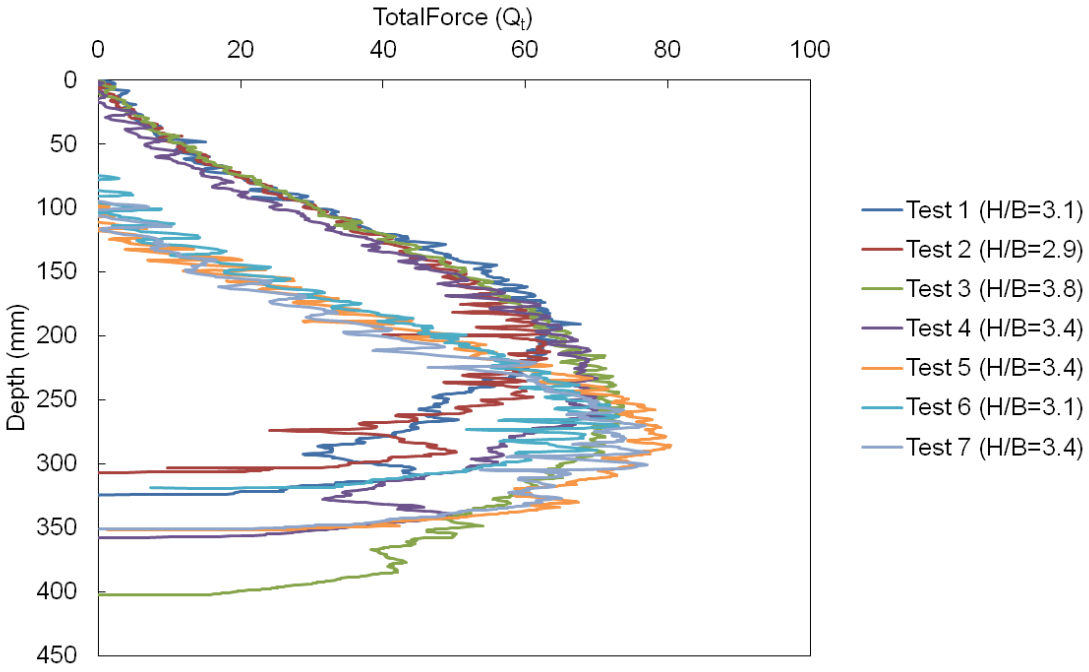

Figure 52. Results of the in-plane (vertical fluke) upward tests.

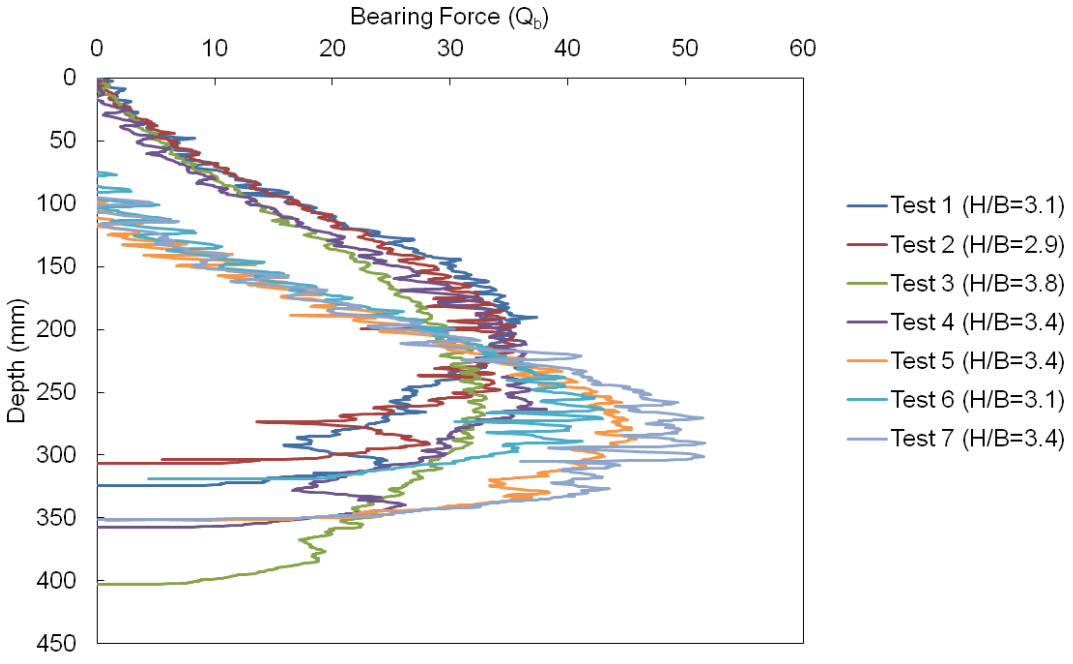

Figure 53. Results of the in-plane (vertical fluke) upward tests.

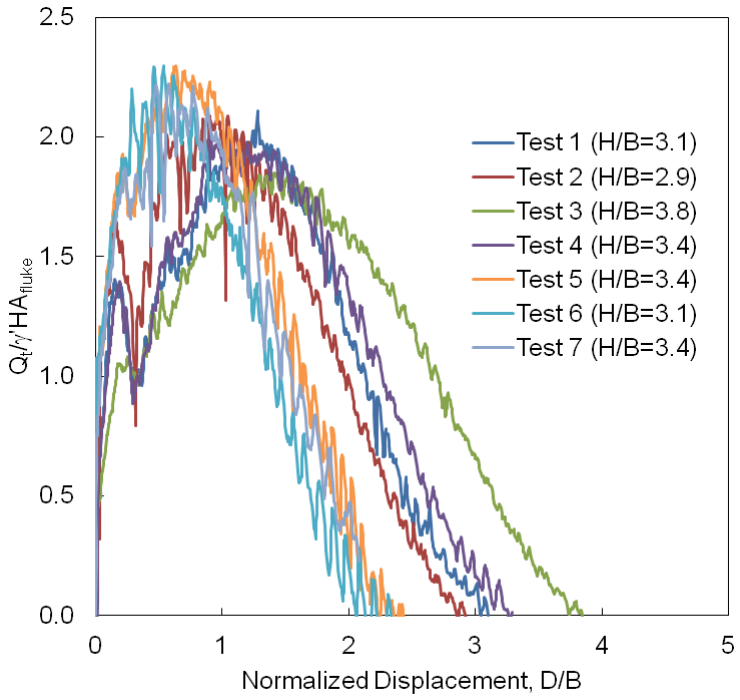

Figure 54. Normalized results of the in-plane (vertical fluke) upward tests.

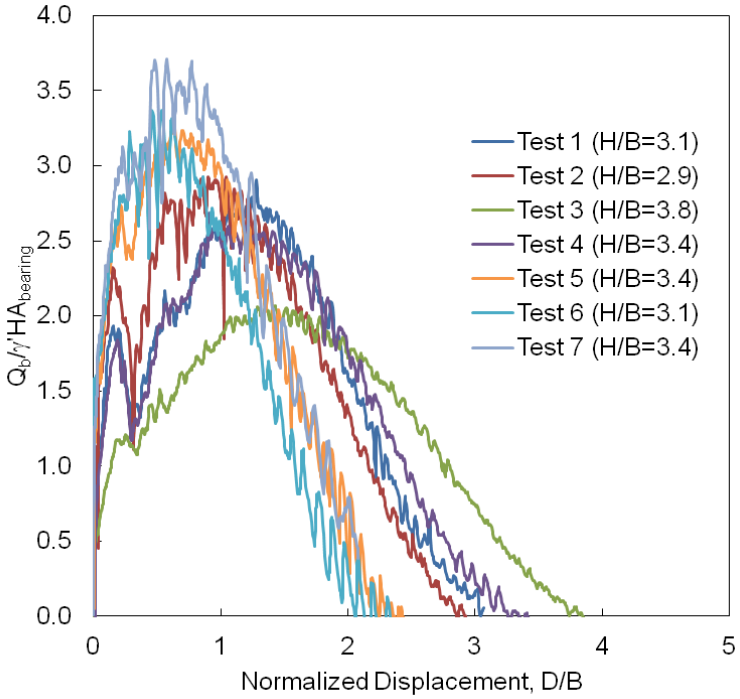

Figure 55. Normalized results of the in-plane (vertical fluke) upward tests.

Table 4. Summary of bearing factors (Equation 13) for the in-plane (vertical fluke) upward tests.

Test	1	2	3	4	5	6	7	Average
H/B=3	2.1	2.1	-	2	2.3	2.3	2.2	2.2
H/B=4	-	-	1.9	-	-	-	-	1.9

4.2.3 DISCUSSION

The displacement or drag distance of the upward tests ranged from 404 to 158 mm. The uplift started at the embedment depth equal to the penetration depth achieved in the downward test. The anchors were then pulled continuously upward, and so the displacement results are presented in Figures 54 and 55 as embedment ratios (D/B).

The capacities of the tension test are all in the same range. All tension tests showed an early peak and a softening of the graph after the peak. The anchors reached their peak capacity with displacement in the range of 90 to 150 mm for tests 1 through 4 and 48 to 66 mm for tests 5 through 7. That means it reached the peak about a displacement ratio D/B=1 for test 1 to 4 (about H/B=2), while tests 5 through 7 reaches the peak significantly less than D/B=1 (about H/B=1). The softening occurs because of the reduction in soil overburden and confining pressure as the anchor is pulled out.

The bearing factors (Equation 13) appear to decrease slightly with increasing embedment ratio ranging from 2.2 at an H/B=3 down to 1.9 at an H/B=4. Again these values appear to be relatively independent of the embedment depth because the bearing factor is accounting for the increase in resistance from the overburden stress. However, the values are smaller than in downward because the bearing resistance is being provided by the top of the anchor that has a more streamlined shape and is at a much shallower depth than the anchor tip at the same embedment ratio.

4.3 NORMAL (VERTICAL FLUKE) TESTS

This section presents the results of the normal (vertical fluke) tests.

4.3.1 CALCULATIONS

The load was calculated by multiplying the calibration factor of the load cell with the load cell readings. The 2224 N (500 lbs) and the 11121 N (2500 lbs) load cell were used for the tests. The calibration factor for the 2224 N (500 lbs) load cell is 70.32 N/mV (15.81 lbs/mV) and for the 11121 N (2500 lbs) load cell is 333.33 N/mV (74.94 lbs/mV). The calibration factors are positive during pull. The string potentiometer was measured in inches. The program i100 instruNet was used to read load and displacement data.

For each test a non-dimensional bearing factor were calculated as well. The bearing factors were calculated for the total resistance at failure (Q_{tu}), which combines shear and bearing, and concentrates on the fluke area of the anchor. It was assumed that the resistance is 100% bearing. The $Q_t/\gamma'HA_{fluke}$ curves were calculated with a fixed H and a variable Q, and were plotted versus horizontal displacement. The bearing factors were calculated with Equation 13 similar to the in-plane shear (vertical fluke) downward tests. For the normal (vertical fluke) tests the embedment depth did not change or slightly, therefore H is fixed in the bearing factor calculation. The bearing factor was presented versus D/B, which is the horizontal drag distance over anchor

height.

To calculate the bearing percentage of the anchor, the same procedure as for the in-plane shear (vertical fluke) downward test (without rod calculations) was used. It was determined that the resistance was primarily from end bearing. Therefore Q_{tu} and $N\gamma$ was assumed to be 100% bearing. The fluke area for the bearing factors (Equation 13) was calculated with Equation 22.

4.3.2 RESULTS

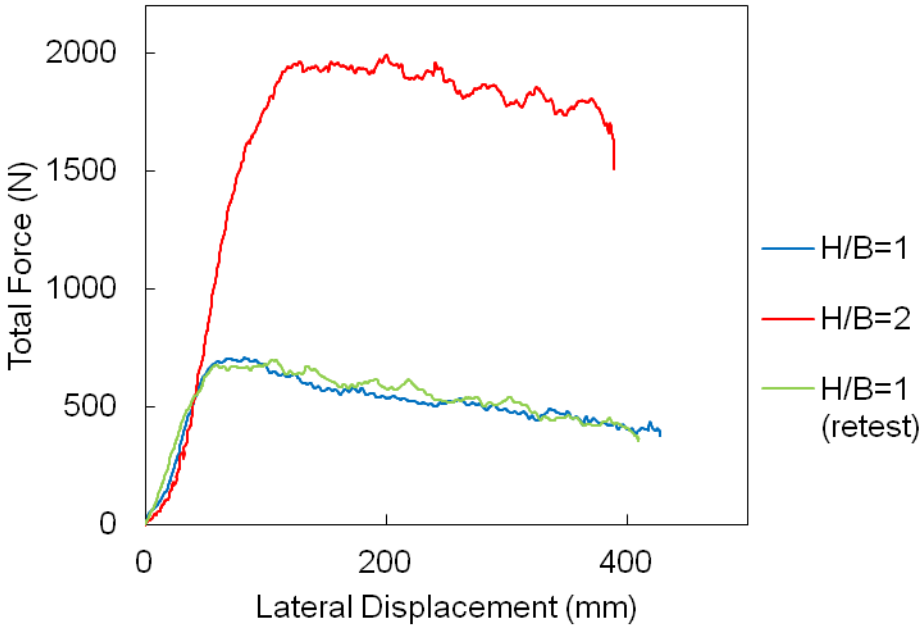

Figure 56. Results of the normal (vertical fluke) tests.

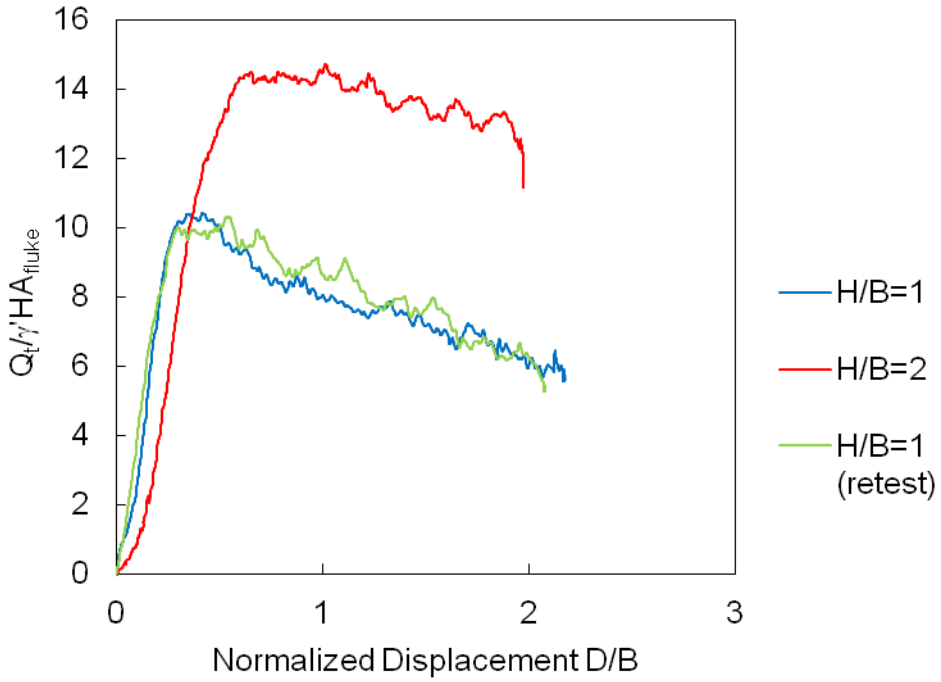

Figure 57. Normalized results for the normal (vertical fluke) tests.

Table 5. Summary of bearing factors (Equation 13) for normal (vertical fluke) tests.

Test	1	2	3	Average
H/B=1	10.42	-	10.32	10.4
H/B=2	-	14.69	-	14.7

4.3.3 DISCUSSION

The displacement or drag distance of the normal (vertical fluke) tests ranges from 400 to 430 mm. No significant shear percentage was determined for all tests as mentioned before (i.e. about 1%); therefore the resistance and bearing factors are considered to be 100% bearing.

The resistance of the normal (vertical fluke) tests showed an early peak and a softening of the graph after the peak. The softening occurs because it reflects the dilative nature the soil in the test tank that would exhibit strain softening behavior at the low confining pressure levels in the test tank. Also, the anchor started to pull out of the soil at large displacements that would reduce the resistance from loss of embedment.

The two tests at H/B=1 were very repeatable showing almost identical resistance curves. By comparing the embedment depth H/B= 1 to 2, it can be observed that the anchor in H/B=1 reaches peak capacity at lower displacements then at H/B=2. The H/B=1 tests reaches their peak before a displacement ratio of D/B=1, while the H/B=1 test reaches the peak slightly after D/B=1.

The bearing factor corresponds to the peak normalized resistance in Figure 57. The bearing factor ranged from 10 at an H/B=1 to 15 at H/B=2. Conceptually the resistance is due to the net lateral earth pressure (i.e. difference between the passive and active earth pressures). At shallow embedments (i.e. H/B=1) the soil is undergoing

a wedge type failure where the failure surface extends from the bottom of the anchor to the soil surface. However, as the embedment goes up the anchor is transitioning towards a more localized “deep” failure mechanism that results in a higher bearing factor.

Figure 58. Photograph of the anchor model upwards movement during the normal (vertical fluke) test at H/B=1.

4.4 PITCH ROTATION (VERTICAL FLUKE) TESTS

This section presents the results of the pitch rotation (vertical fluke) tests.

4.4.1 CALCULATIONS

The moment was calculated by multiplying the calibration factor of the torque sensor with the torque sensor readings. The calibration factor for the 226 Nm (2000 lbs-in) torque sensor is 11.44 Nm/mV (101.26 lbs-in/mV). The capacity of the torque test has to be adjusted because of the friction on the rod. The rod was tested separately in an embedment depth for H/B=1, 2 and 3 and the maximum torque was measured. For the H/B=1 the friction is about 0.665 Nm (5.89 lbs-in), the H/B=2 is about 0.869 Nm (7.69 lbs-in), and the H/B=3 is about 0.917 Nm (8.12 lbs-in). The test data were adjusted to remove the rod friction.

The tracking device reads in Euler degrees (pitch, yaw and role). The program i100 instruNet was used to read moment data and the Polhemus program to read to Euler angles

For each test a non-dimensional bearing factor was calculated. The bearing factors were calculated for the total torque resistance at failure (T_u), which combines shear and bearing and concentrates on the bearing area of the anchor. For the pitch rotation (vertical fluke) tests the N_γ was calculated by using T_u, the deepest H and the square

root of the fluke area A as the lever arm (see Equation 25). The $T/\gamma' HA_{fluke}L$ curve was calculated with a variable T and a fixed H and L. The square root of the fluke area was used for L because it is assumed that it is equivalent to a square fluke area, so the lever arm is not depended on the geometry of the fluke. T_u is the ultimate moment (bearing and shear). As seen on Equation 25 the lever arm (square root of the fluke area) was added to the Equation 13, because of the moment.

$$N_\gamma = \frac{T_u}{\gamma' H A_{fluke} L} \tag{25}$$

Where T_u is the maximum torque, A is the fluke area, and L is the length of an equivalent square fluke. The pitch rotation (vertical fluke) was anticipated to be controlled mainly by bearing on the fluke. Therefore T_u and N_γ was assumed to be 100% bearing. The fluke area was calculated with Equation 22.

4.4.2 RESULTS

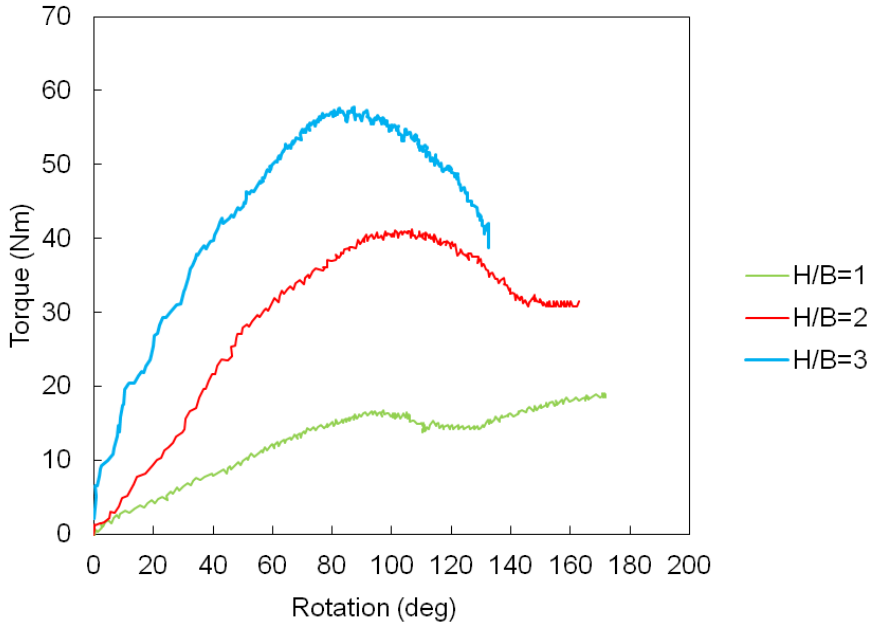

Figure 59. Results of the pitch rotation (vertical fluke) tests.

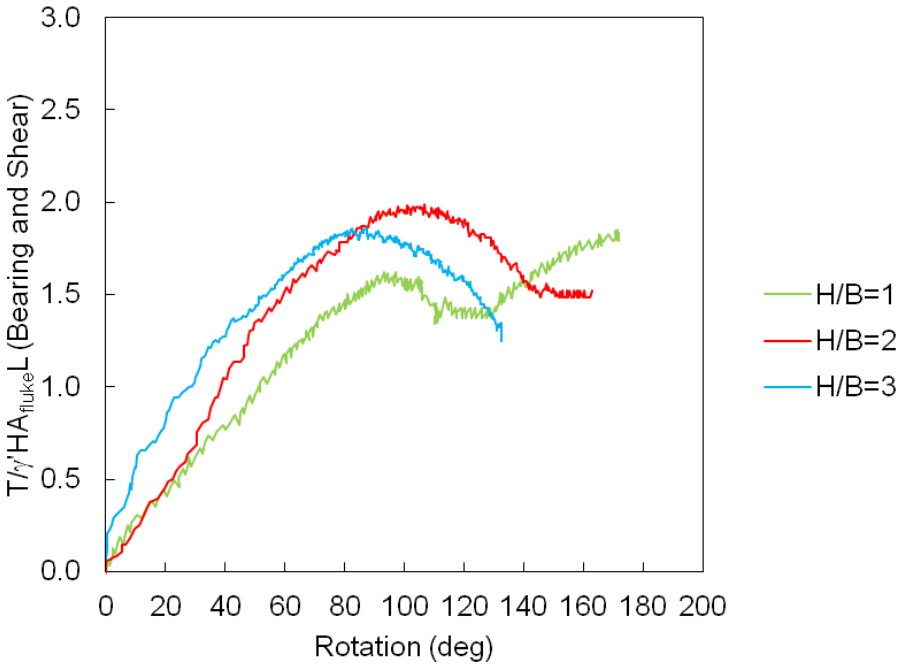

Figure 60. Normalized results for the pitch rotation (vertical fluke) tests.

Table 6. Summary of bearing factors (Equation 13) for the pitch rotation (vertical fluke) tests.

Test	1	2	3	Average
H/B=1	1.855	-	-	1.9
H/B=2	-	1.99	-	2
H/B=3	-	-	1.86	1.9

4.4.3 DISCUSSION

The rotation angles of these test ranged from 132 to 172 degrees. The pitch rotation tests showed a significant capacity peak and a softening afterwards, i.e. the capacity increases, reaches a peak and decreases after the peak. In H/B=1 the capacity increases again after it reaches an initial peak. This can be seen on Figure 59, where the torque reaches a peak, fails and increases after that with increasing angle. This can be explained due the shallow embedment the sand surface collapse during the rotation, so the mobilized soil wedge increases until the anchor is almost horizontal and after the 90° rotation the soil mobilization behavior repeats (Figure 61). This behavior was not observed in the deeper embedment tests.

The capacity of the test at H/B=2 and 3 reaches a peak followed by softening. It is anticipated that the soil is flowing locally around the anchor during rotation and thus reflects the strain-softening stress-strain behavior of the soil in the test tank. The bearing factors were approximately constant ranging from 1.7 for H/B=1 to 2 for H/B=3. In this mode of failure the resistance is being controlled by the shear strength of the soil locally around the anchor, which should increase approximately linearly with depth. The normalization of stress therefore is accounting for this effect resulting in approximately constant bearing factors with depth.

Figure 61. Photograph of the failure surface from the H/B=1 test after rotation.

4.5 IN-PLANE SHEAR (HORIZONTAL FLUKE) TESTS

This section presents the results of the in-plane shear (horizontal fluke) tests.

4.5.1 CALCULATIONS

The load was calculated by multiplying the calibration factor of the load cell with the load cell readings. The 890 N (200 lbs), 2224 N (500 lbs), and 11121 N (2500 lbs) were used for the tests. The calibration factor for the 890 N (200 lbs) load cell is 28.3 N/mV (6.369 lbs/mV), for the 2224 N (500 lbs) load cell is 70.32 N/mV (15.81 lbs/mV), and for the 11121 N (2500 lbs) load cell is 333.33 N/mV (74.94 lbs/mV). The calibration factors are positive during pull. The string potentiometer was measured in inches. The program i100 instruNet was used to read load and displacement data.

For each test a non-dimensional bearing factor was calculated as well. The bearing factors were calculated with Equation 13 and 14 similar to the in-plane shear (vertical fluke) downward tests. The $Q_t/\gamma'HA_{fluke}$ and $Q_b/\gamma'HA_{bearing}$ curves were calculated with a fixed H and a variable Q, and were plotted versus horizontal displacement.

To calculate the bearing percentage of the anchor, the same procedure as for the in-plane shear (vertical fluke) downward test was performed. The vertical effective stress was used to calculate the shear force, because the anchor lay horizontally in the sand

bed. The shear force is calculated with Equation 15 to estimate the shear percentage and therefore also the bearing percentage of the tests. The shear area of the anchor was calculated with Equation 20. A significant percentage of shear could be determined for all tests, therefore the bearing factors were calculated separately for total and bearing resistances.

The fluke area for the bearing factors (Equation 13) was calculated with Equation 22 and the bearing area for the bearing factor (Equation 14) was calculated from the following:

$$A_{bearing} = ad_{anchor}2 \quad (26)$$

where a is the bottom side length of the anchor and d_{anchor} is the thickness of the anchor.

4.5.2 RESULTS

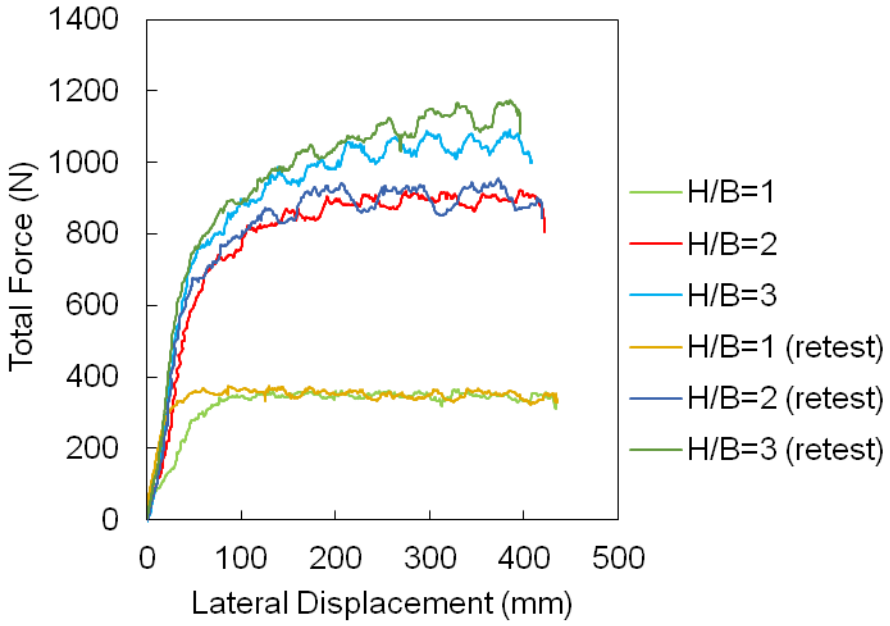

Figure 62. Results of in-plane shear (horizontal fluke) tests.

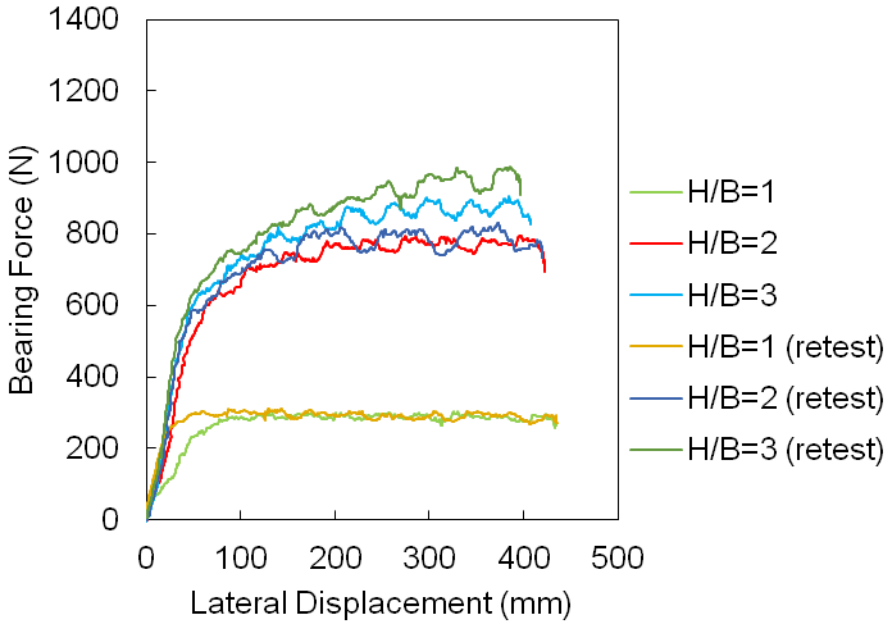

Figure 63. Results of in-plane shear (horizontal fluke) tests.

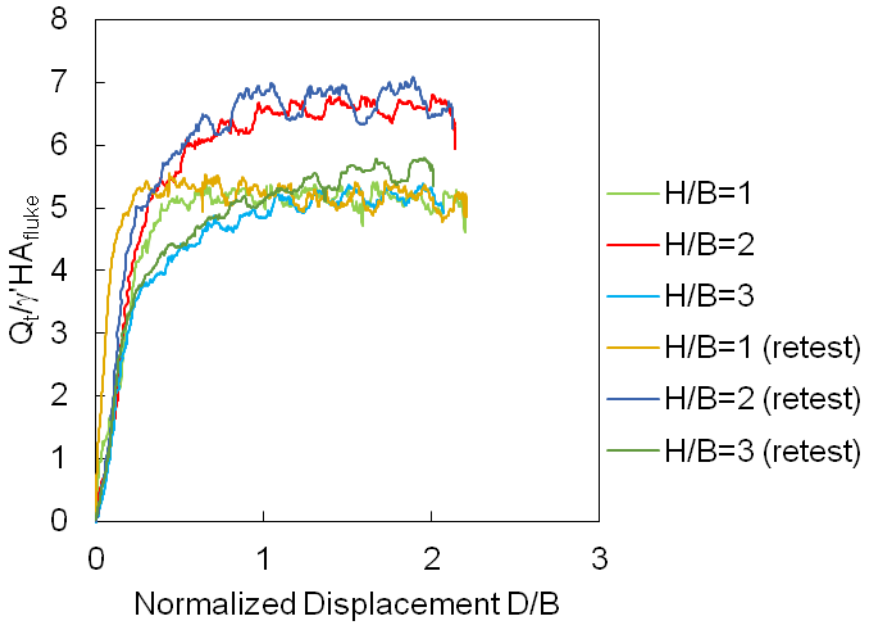

Figure 64. Normalized results of in-plane shear (horizontal fluke) tests.

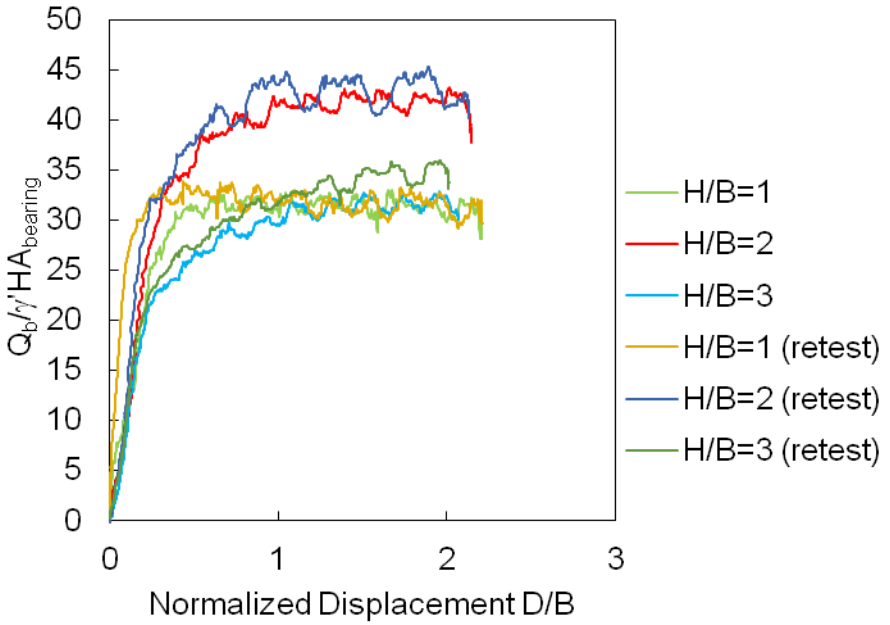

Figure 65. Normalized results of in-plane shear (horizontal fluke) tests.

Table 7. Summary of bearing factors (Equation 13) for in-plane shear (horizontal fluke) tests.

Test	1	2	3	4	5	6	Average
H/B=1	5.4	-	-	5.6	-	-	5.5
H/B=2	-	6.8	-	-	7	-	6.9
H/B=3	-	-	5.4	-	-	5.8	5.6

4.5.3 DISCUSSION

The tests showed an early peak and no softening afterwards as shown in Figure 62 and 63. The reason for that is due the position of the anchor on the sand bed; it can be dragged completely horizontal without any rotational movement and the overburden stress remains constant on the anchor.

Retests were performed at all embedment ratios with different load cells and the test results were similar. The initial test and retest showed almost identical curves with slightly different peak capacities. It was observed that the peak capacity of the H/B=2 test was slightly lower than of H/B=3 test, while the H/B=1 test showed a significantly lower capacity than the other embedment depths. The anchor with the lowest embedment depth reached peak capacity at the smallest displacement. The test showed that with increasing embedment depth, the capacity increases slightly. All 6 tests reach their peak almost at the same drag displacement, which ranged from 50 to 60 mm.

The normalized resistance showed the same behavior as the curves of the displacement versus load. The bearing factors (Equation 13) ranged from 5.5 to 6.9. All curves show the same behavior. The H/B=3 tests showed the lowest bearing factors but increases over the H/B=1 curve after a certain distance. The bearing factors for H/B=2 were the highest of all embedment depths.

In the in-plane shear (horizontal fluke) mode of failure the resistance is being controlled mostly by the net passive resistance of the soil with some resistance due to

interface friction. The friction should increase linearly with embedment depth and thus normalization should account for this effect. Given that the plate is thin relative to the embedment depth it is anticipated that the bearing failure is localized and thus the resistance should be controlled by the shear strength in the vicinity of the anchor tip. The normalization should result in an approximately constant bearing factor with depth that is more or less consistent with the observations.

4.6 SUMMARY

A summary of average bearing factors for all loading modes is presented in Table 8. Only the bearing factor (Equation 13) values are used because this is what will be used initially in the simplified kinematic modeling approach in Gilbert et al. (2013) and Huang (2015). As shown in the table the highest bearing factors can be seen in the in-plane shear (vertical fluke) direction, followed by the in-plane shear (horizontal fluke) direction, followed by the normal (vertical fluke) direction. The bearing factors were significantly smaller in the in-plane shear (vertical fluke) upward and pitch rotation directions.

The trends in bearing factors can be explained by the resistance mechanism. Three of the loading modes were likely controlled by a local "deep" failure mechanism. For example, in the in-plane shear (vertical fluke and horizontal fluke) modes, the bearing area is much smaller than the embedment depth, which resulted in a localized failure near the tip of the anchor. This is controlled mainly by the shear strength of the soil near the tip of the anchor. In the pitch rotation (vertical fluke) mode the resistance is from soil flowing around the anchor and thus controlled by the shear strength of the soil locally around the anchor. Since shear strength increases linearly with embedment depth the normalization results in an almost constant bearing factor with depth. An exception is the normal (vertical fluke) mode, where the bearing factors increased with depth. This is likely attributed to a transition from a shallow wedge type failure to a deeper flow type failure as the embedment ratio increases.

Table 8. Summary of the average bearing factors (Equation 13) under pure loading at various embedment ratios.

H/B	In-plane shear (vertical fluke) downward	In-plane shear (vertical fluke) upward	Normal (vertical fluke)	Pitch rotation (vertical fluke)	In-plane shear (horizontal fluke)
1	18.3	-	10.4	1.9	5.5
2	17.4	-	14.7	2	6.9
3	15.7	2.2	-	1.9	5.6
4	-	1.9	-	-	-

CHAPTER 5: SUMMARY AND CONCLUSIONS

5.1 SUMMARY

The objective of this thesis was to investigate the static resistance of the Flying Wing Anchor under pure loading conditions. The data will be useful for future efforts to model and predict the trajectory of the anchor under service loading. The focus was on four pure loading modes including in-plane shear (vertical fluke), normal (vertical fluke), pitch rotation (vertical fluke) and in-plane shear (horizontal fluke). Pure static loading tests were performed on small-scale models of the Flying Wing Anchor in sand. This included in-plane shear (vertical fluke), normal (vertical fluke), pitch rotation (vertical fluke), and in-plane shear (horizontal fluke). The sand was placed in a rigid test tank by dry pluviation to a relative density of 20%, which corresponds to a prototype relative density of about 35%. In total 14 test tanks were prepared and a total of 26 anchor tests were performed.

5.2 CONCLUSIONS

Following conclusions can be made:

- The literature suggests that the trajectory of an embedded plate anchor can be determined through the determination of its resistance under pure loading.

- The following bearing factors were determined for the Flying Wing Anchor for embedment ratios of 1 to 3: 16 to 18 for in-plane shear (vertical fluke) downward, 2 for in-plane shear (vertical fluke) upward, 10 to 15 for normal (vertical fluke), 2 for pitch rotation (vertical fluke) and 6 to 7 for in-plane shear (horizontal fluke).

- With the exception of the normal (vertical fluke) mode, all other loading modes appear to be controlled by a localized bearing failure mode, and normalizing the resistance by the overburden stress is resulting in a bearing factor that is more or less constant with depth.

5.3 RECOMMENDATIONS AND FURTHER STUDIES

The University of Texas has recently developed a model for predicting the trajectory of the Flying Wing Anchor in clay (Gilbert et al., 2013 and Huang, 2015), where they use bearing factors from various penetration modes to model the trajectory. This model could be modified for the analysis of anchors embedded in sands that would utilize the bearing factors from the results of this thesis.

Tests in deeper embedment depths, i.e. greater than H/B=3, do not have to be carried out for now. The reason for that is that Breithaupt (2015) showed that by testing the dynamic free-fall penetration, the maximum penetration in dry sand is H/B=3 for the Flying Wing Anchor. The Flying Wing Anchor potentially penetrates the soil deeper than plate anchors. It starts deeper than the maximum drag depth of drag anchors and dives twice as deep during drag.

This research was carried out for loose sand with a relative density of about 20%. Future research could also investigate bearing factors in dense sand including the development of theoretical bearing factors that would incorporate fundamental soil properties.

BIBLIOGRAPHY

ASTM Standard (2007); Test method for particle-size analysis of soils. *ASTM international, West Conshohocken, PA, DOI: 10.1520/D4513-11*

ASTM Standard (2006a); test methods for maximum index density and unit weight of soil using a vibratory table. *ASTM international, West Conshohocken, PA, DOI: 10.1520/D4253-00R06*

ASTM Standard (2006a); test methods for maximum index density and unit weight of soil and calculations of relative density. *ASTM international, West Conshohocken, PA, DOI: 10.1520/D4254-00R06E1*

Bradshaw, A.S., Giampa, J., Dietrich, F., Gilbert, R. and Gerkus, H. (2014); Pullout capacity of plate anchors in sand for floating offshore wind turbines. *ISFOG*

Breithaupt, B. (2015): The dynamic Penetration of Flying Wing anchors (Patent Pending): *Master Thesis, Civil and Environmental Engineering, University of Rhode Island, Kingston.*

Butterfield, S. and Musial, W. (2004); 'Future for Offshore Wind Energy in the United States: Preprint'

Dietrich, F.C. (2014); Evaluation of theoretical capacity models for plate anchors in sand in relation to floating offshore wind turbines. *Master thesis, University of Rhode island, Kingston, Rhode Island.*

Gade, V.K., Dave, T.N., Chauhan, V.B. and Dasaka, S. (2013); Portable Traveling Pluviator to reconstitute specimens of cohesionless soils

Giampa, J.R. (2014); Interpretation of shallow helical anchor capacity in sand. *Master thesis, University of Rhode island, Kingston, Rhode Island.*

Gilbert, R. and Bradshaw, A.S., (2012); Green Foundations for Green Energy. *Research Proposal Submitted tot he National Science Foundation.*

Gilbert, R., Gerkus, H., Iturriaga, E., and Vilkki, J., (2013); Initial Embedment of Drag Embedment Anchor and Vertically Loaded Anchor Models-Initiation of Movement. *Report I, University of Texas at Austin, Department of Civil, Architectural, Environmental Engineering, Geotechnical Engineering*

Hibbler, R.C. (2008); Mechanics of Material. *seventh edition, published by Pearson Prentice Hall*

Huang, Y., (2015); Designing a Laboratory Model Test Program for Developing a New Offshore Anchor. *Master thesis, University of Texas at Austin*

Le Lievre, B., and Tabatabaee, J. (1981); The performance of marine anchors with planar flukes in sand; *Canadian Geotechnical Journal, 18: 520-534*

Liu, H., Li, Y., Yang, H., Zhang, W., and Liu, C. (2010a); Analytical study on the ultimate embedment depth of drag anchors. *Ocean Engineering, 37(14-15), 1292-1306.*

Liu, H., Zhang, W., Zhang, X., and Liu, C. (2010b); Experimental investigation on the penetration mechanism and kinematic behavior of drag anchors. *Appl. Ocean Res. 32 (4), 434-442.*

Liu, H., Liu, C., Yang, H., Li, Y., Zhang, W., Xiao, Z. (2012a); A novel kinematic model for drag anchors in seabed soils. *Ocean Engineering, 59, 33-42.*

Liu, H., Zhang, W., Liu, C., and Hu, C. (2012b); Movement direction of drag anchors in seabed soils. *Appl. Ocean Res., 34, 78-95.*

Matha, D. (2009) 'Model Development and Loads Analysis of an Offshore Wind Turbine on a Tension Leg Platform with a Comparison to Other Floating Turbine Concepts: *April 2009', NREL.*

Matha, D, Fischer, T. and Kuhn, M. (2009) 'Model Development and Loads Analysis of an Offshore Wind Turbine on a Tension Leg Platform'.

Miedema, S.A., (1987); Calculation of the Cutting Forces when Cutting Water Saturated Sand. *September 1st*

Musial, W. and Butterfield, S. (2004) 'Future for Offshore Wind Energy in the United States: Preprint'. NREL.

Musial, W., Butterfield, S., and Boone, A. (2004); Feasibility of floating platform systems for wing turbines. *23rd ASME Wind energy symposium, NREI, Reno, Nevada.*

NAVFAC (ed.), (2012) Handbook for Marine geotechnical Engineering, NAVFAC, Port Huneme, California.

Neubecker, S.R., and Randolph, M.F. (1996b); The static equilibrium of drag anchors in sand. *Canadian Geotechnical Journal, 33: 574-583*

Neubecker, S.R., and Randolph, M.F. (1996a); The kinematic behaviour of drag anchors in sand. *Canadian Geotechnical Journal, 33: 584-594*

Randolph, M.F. and Gourvenec, S. (2011); Offshore geotechnical engineering. *1st ed, Spon Press, Abingdon, Oxon, New York, NY.*

Ruinen, R., and Degenkamp, G., Vryhof Anchors B.V. (2002); OTC 14305 – Prediction of the Holding Capacity and Trajectory of Drag Embedment Anchors

TU Delft; M. van den Hatert, B. Jonkman, D. Strijbis (2005); Penetration behavior of an anchor in sand

Verruijt, A., (1983); Grondmechanica. *Delftse uitgevers maatschappij, Nederland*

Vrihof anchors (2010); Anchors manual 2010. *Vrijhof anchors b.v. Capelle a/d Yssel, the Netherlands*